UNIVERSITAT POLITÈCNICA DE VALÈNCIA

ESCUELA TÉCNICA SUPERIOR INGENIEROS INDUSTRIALES VALENCIA

TRABAJO FIN DE MASTER EN INGENIERÍA BIOMÉDICA

DESIGN OF A NON-INTRUSIVE SYSTEM FOR NEONATES MONITORING

AUTHOR: ROBERTO HERRERO FELTRER

SUPERVISOR: JAVIER CALPE MARAVILLA

Academic year: 2018-19

Agradecimientos

Tardó pero, al fin, llegó el momento de escribir unas líneas en esta página. Antes que nada, me gustaría agradecer a Javier Calpe su inestimable ayuda en todo momento durante el desarrollo de este trabajo, así como a los compañeros del laboratorio de aplicaciones Sergio y Juan Fran. Tampoco me olvido de Abraham, mi compañero de cueva, y de Álex, por los consejos y los descansos a las 3.

A mis compañeros del Máster que conocí hace ya un par de años y que han acabado convirtiéndose en amigos: Íñigo, Ana, Violeta, Cristina, Xesco, Leo y Matías (al que le tengo que agradecer muchas tardes de redacción y de dudas). Y a Amanda, por animarme a embarcarme en este proyecto y, sobre todo, por ser como fuiste.

A Borja y Nacho, mis mejores amigos. Gracias por la amistad incondicional, por vuestros consejos, por los ánimos y por el apoyo en los momentos más complicados.

A mi familia. A mi yayo y a mi yaya, por ser ejemplos de amor, de duro trabajo, fuerza y superación hasta en el mayor de los desalientos. A mis tres tíos Merche, Raúl y Jose Luís, por ser fuente de inspiración. A mis primos pequeños Edu, Carmen, Miquel y, a la nueva de la família, Emilia, por recordarnos que el tiempo es imparable y que la vida se abre paso.

Y por último, a las personas más importantes de mi vida. Agradecido a mi hermano, por ser el primer amigo que hice y por ser la referencia que siempre tuve, desde el momento en que nací. A mi padre, por su constante dedicación y lucha diaria hasta en los momentos de mayor flaqueza. Y a mi madre, por su bondad, por superarse y reinventarse cada día, y por mostrarme el camino en mis más oscuros días.

Abstract

Neonates, especially pre-term neonates, are a sensitive population that may require continuous vital sign monitoring. It is highly advisable to provide this monitoring in a non-invasive or, even better, non-intrusive way, thus facilitating interaction with parents and doctors.

We will explore the use of standard video cameras to measure two most relevant signs, heart rate (HR) and breathe rate (BR). Additionally the system may monitor breathe dynamics and allow visual monitoring and tracking of neonate motion.

The system will consist of a stereo pair so depth images may be obtained. So we will need to specify and design the system to obtain the required specifications (mainly depth resolution and field of view)

We will need to calibrate the cameras using an integrating sphere and the stereo pair using a variation of Hirschmuller algorithm in order to obtain reliable information. From those corrected images HR and BR will be extracted.

Images are acquired at the Neonatologist Unit in the Hospital General de Valencia where we obtained the approval from the ethics committee and there is a collaboration with the medical doctors.

Results will be discussed and further actions outlined.

Keywords: neonates, monitoring, heart rate, breathing rate, signal processing, biomedical engineering, rgb, calibration experiments, stereo pair, depth.

Resumen

Los neonatos, especialmente los prematuros, son una población sensible que puede requerir una monitorización continua de los parámetros vitales. Es muy recomendable realizar esta monitorización de forma no invasiva o, mejor aún, no intrusiva, facilitando así la interacción con los padres y los médicos.

Exploraremos el uso de cámaras de vídeo estándar para medir dos de los signos más relevantes, la frecuencia cardíaca (HR) y la frecuencia respiratoria (BR). Además, el sistema puede monitorizar la dinámica de la respiración y permitir la monitorización visual y el seguimiento del movimiento del neonato.

El sistema consistirá en un par estereoscópico para poder obtener imágenes de profundidad. Por tanto, tendremos que especificar y diseñar el sistema para obtener las especificaciones requeridas (principalmente resolución de profundidad y campo de visión).

Necesitaremos calibrar las cámaras utilizando una esfera integradora y el par estéreo utilizando una variación del algoritmo de Hirschmüller para obtener información fiable. De las imágenes corregidas se extraerán los valores de HR y BR.

Las imágenes se adquieren en la Unidad de Neonatología del Hospital General de Valencia donde se obtiene la aprobación del comité de ética y se colabora con los médicos.

Se discutirán y comentarán los resultados y se propondrán nuevas acciones.

Palabras Clave: neonatos, monitorización, frecuencia cardíaca, frecuencia respiratoria, procesamiento de señales, ingeniería biomédica, rgb, experimentos de calibración, par estéreo, profundidad.

Collaborative framework

This work has been done within the *NEO9TEC* project *Early diagnosis of neonatal sepsis by monitoring cardiac variability*, file *12-NEO9TEC-CALPE-LURBE-2017-B* in the call for *VLC_Bioclinic* in the year 2017.

Contents

List of Figures

List of Tables

Part I

Report

Chapter 1

Introduction

1.1 State-of-the-art

1.1.1 Medical context

Neonates

In 2016, the neonatal mortality in developed countries was 2.3 per 1000 live births according to The Organisation for Economic Co-operation and Development (OECD). Neonates are babies 4 weeks of age or younger. They can range from babies born in the normal period (9 months) to babies born prematurely a few months earlier. Therefore, they are in a very early stage of life and many of them are premature to face the next stages (Kliegman 2015). They are at a point where they need a lot of specialized care and a high level of attention because any small change or alteration in them can have very serious consequences. Currently, the three most common causes of neonatal deaths are respiratory diseases (such as respiratory distress syndrome), infections (such as sepsis) and birth asphyxia; they might represent 80% of global neonatal deaths (WHO n.d.). Some of the most prominent symptoms in these diseases are slow heart rate, rapid breathing rate, or brief stoppage of breathing (apnea). Early diagnosis of infections would help, through appropriate treatment, to reduce neonatal mortality. For this reason, it is necessary to follow observation procedures and to have the required tools in neonatal units to make a protocol for the follow-up and monitoring of certain vital signs such as heart rate or respiratory rate. Currently, the monitoring systems used in neonatal units are the traditional ones, such as the electrocardiograph and the pulse oximeter. With the first one, direct parameters such as the electrocardiogram signal (ECG) captured by heart's electrical activity, and indirect parameters such as heart rate or breathing rate can be extracted (Valderas et al. 2015). With the second one it is possible to know the oxygen saturation in the blood. These systems are widely installed in all hospitals and although they are not invasive, they are somewhat intrusive for newborns as they are in contact with the skin and may cause some damage and discomfort in them. In addition, it can also be annoying for the relatives or people in charge of the newborns. It should be remembered that the conditions of some neonates can be very delicate and the fact of using intrusive systems can

generate significant levels of stress in the people in charge of them. It may therefore be interesting to investigate alternatives to traditional systems by trying to find one that is less intrusive or non-intrusive in which the comfort of the neonates is as high as possible and, in turn, is able to assist in the monitoring of vital signs.

Heart Rate

The heart is a set of muscles responsible for pumping blood to the tissues in order to provide them with the nutrients necessary for physiological activity. This group consists of the ventricular muscle, the atrial muscle and the conductive muscle fibers. They are in charge, by means of ionic exchange mechanisms, of performing cardiac cycles, which have a temporary duration from the beginning of one heartbeat until the beginning of the next one. In other words, the cardiac cycle consists in the occurrence of a period of blood heart filling called diastole and of a period of contraction called systole (Guyton and Hall 2011a). In cardiac events, several changes in physiological parameters are described as shown in figure 1.1. The study of changes in some

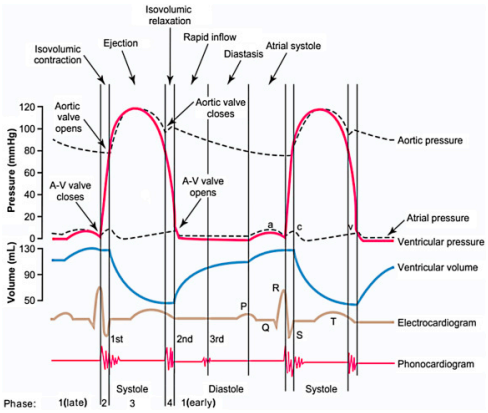

Figure 1.1: Cardiac events for left ventricular function (Guyton and Hall 2011a).

of these parameters is essential to describe the causes of many diseases and, in turn, to study other derived parameters such as heart rate (HR). HR is the frequency of the heartbeat, i.e, it determines the number of times the heart beats in a given time. Normally, the value of this parameter is expressed in beats per minute. Depending on the value, HR can determine normal or abnormal rhythms. Regarding the HR values, the range of values defined for normal activity in healthy adults is from 60 to 100 beats per minute (*bpm*), although these values can be variable, especially under certain situations. For example, if a person is resting and his HR is 90 or 100 bpms, this could suggest a certain abnormality in his cardiac rhythm despite being within the established range (Spodick 1992). Thus, these values are the threshold for fast HR abnormal rhythm like tachycardia or slow HR abnormal rhythm like bradycardia. Diseases directly related to abnormal sinus rhythms include bradycardia (whose values are less than 60 bpms), tachycardia (whose values are higher than 100 bpms), and sinus arrhythmia (that produces a 30% increasing or decreasing during a deep respiration) (Guyton and Hall 2011b). Figure 1.2 shows two of the mentioned arrhythmias. In neonates, the HR values are different: the range is from 90 to 165 bpms (Kliegman 2015). Another important parameter is heart rate variability (HRV). It describes the changes in HR values in a given time interval. Therefore, if the values of the HR remain constant in that interval, the variability will be very small. An example of this would be a person at

rest without any pathology. In case the HR values are very different in the time interval the variability will be high. An example of this would be a person suffering an arrhythmic event, such as tachycardia or fibrillation.

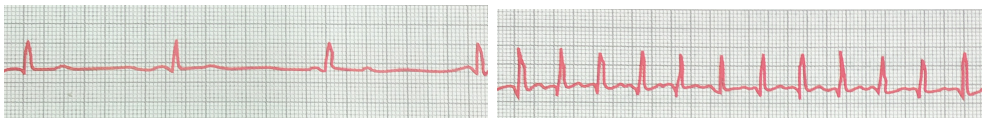

(a) Bradycardia ECG signal **(b)** Tachycardia ECG signal

Figure 1.2: Abnormal sinus rhythms.

Breathing Rate

The lungs are two organs that lie on either side of the middle space of the rib cage. They produce the exchange of carbon dioxide for oxygen in order to provide it to the tissues and organs that make up the human body. The process of breathing is carried out thanks to mechanisms of expansion and contraction that are produced due to the activation of some muscles. These muscles can be either the diaphragm or the inspiratory or expiratory muscles. In the case of the diaphragm, breathing is achieved by the vertical movement of the diaphragm in both directions. In the case of inspiratory and expiratory muscles, a forward and backward movement of the ribs is provoked, thus increasing the thoracic cavity. Although we are able to control breathing voluntarily, it is mainly controlled by the autonomic nervous system (Russian 2015). In the same way as HR, breathing rate (BR) can also be quantified. BR measures how many times the normal breathing cycle occurs in a given time interval. In healthy adults, this parameter is usually measured in breaths per minute and its values are between 12 and 20 breaths every 60 seconds (Flenady and Dwyer 2016). In neonates, the values are between 30 and 55 breaths every 60 seconds (Kliegman 2015). Table 1.1 summarizes HR and BR ranges.

1.1.2 Technical context

Among the most commonly used systems both in hospitals and at home user level are the traditional ECG monitoring systems, monitoring devices that use the photoplethysmography signal (PPG), and monitoring systems that use the video signal to extract the parameters to be measured. The first one is intrusive and in some cases can be uncomfortable for patients. The last two ones are not intrusive, may be more comfortable for patients but do not provide exactly the same information.

$\mathbf{HR}_{min}$	$\mathbf{HR}_{max}$	$\mathbf{BR}_{min}$	$\mathbf{BR}_{max}$
90	165	30	55

Table 1.1: HR minimum and maximum values in beats per minute (first two columns) of neonates. BR minimum and maximum values in breaths per minute (last two columns) of neonates.

Monitoring systems: ECG signal

One of the most used monitoring systems in the hospital environment is the one that works with the ECG signal. This signal provides information of the electrical activity of the heart and it is very important for the prediction of cardiac diseases such as arrhythmic events after an acute myocardial infarction (Steinberg et al. 1992). Depending on the patient's condition, this type of devices is more or less useful and effective. In addition, depending on which hospital unit it is in, it can be used in one way or another. For example, in the emergency unit the electrocardiograph is used for a few seconds or a few minutes and, if the patient has suffered an acute myocardial infarction, it could be diagnosed through its use. But there are arrhythmias that can only be detected if the monitoring time interval is long. Devices that monitor the ECG signal continuously are called ambulatory ECG monitors and are classified according to duration: short-term, from 24 to 48 hours and long-term from more than 48 hours. Long-term monitors have the disadvantage that they need a lot of memory (Ontario et al. 2017). In the field of home use, there are other devices such as *Kardia Mobile* that calculate the ECG signal from the detected pulse and provide a diagnosis after the measurement by a smartphone application (AliveCor n.d.).

Regarding the extraction of characteristics from the ECG signal, there are some algorithms to extract the HR, such as the Pan and Tompkins one, in which a combination of filters is made to extract the R peaks, which represent ventricular systole and it can be used to generate the HR signal (Pan and Tompkins 1985). Another method is the one developed by *Kutlu and Kuntalp 2010* in which the wavelet package coefficients are used to extract the heartbeat from ECG signals. In addition to HR extraction, there are algorithms that calculate the breathing signal from the ECG signal: commonly known as the EDR signal. The respiratory rate parameter can be extracted from the EDR signal (Valderas et al. 2015). EDR signal is the breathing signal extracted from the ECG signal. According to *Park and Noh* work (Park et al. 2008), the extraction of the breathing signal observed in the figure 1.3 was done in several phases and is based on the idea that the ECG signal is modulated by the breathing signal; when breathing, there is a small displacement of the electrodes with respect to the heart. In the first phase, a preprocessing was done to eliminate power-line noise and baseline wandering. In the next two phases, an R-wave detection and calculation of the area under the curve was made using a moving average filter with a window set as twice the length of the Q and R waves. In the final phases, interpolation was used to reconstruct the breathing signal and low-frequency components of no interest were removed. The results are shown in (figure 1.3).

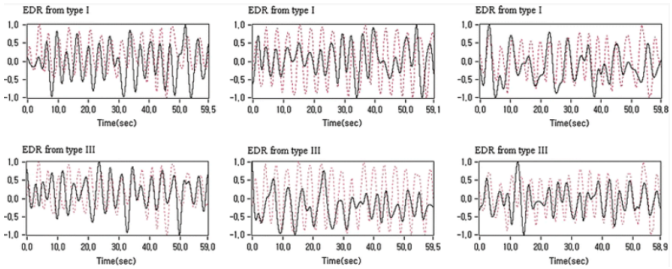

Figure 1.3: Respiration signals extracted by the ECG signals (Park et al. 2008).

Monitoring systems: PPG signal

The PPG signal is obtained by detecting changes in light absorption in tissues. During systole there is an increase in blood volume in the arteries and the light intensity passing through the vessels and received by the sensors is lower. During diastole, the blood volume decreases and, therefore, the light that passes through the tissues and is received by the sensors is greater (Tamura et al. 2014). Apart from the cardiac pulse signal, with this type of device it is possible to measure the oxygen saturation in the blood. This is achieved with red light emitters and near-IR, because depending on the amount of oxygen that is attached to the hemoglobin, the blood-carrying molecule, different wavelengths will be absorbed in different ratios by it. Moreover, after the detection of the HR by means of the PPG signal, algorithms have been developed with which the HRV parameter can be extracted (Foroozan, Mohan, and J. S. Wu 2018). This technique to measure HR is very common in hospitals and other domestic devices. Numerous instruments are used in sport or everyday life that use this technique.

Monitoring systems: Video signal

A different technique for HR extraction is based on color changes in the image. For its development, the acquired video signal is analyzed and processed. In each heartbeat, blood is distributed around the body to the smallest blood vessels. During systole, blood occupies the place established by the vessels to supply nutrients to the tissues. During systole, the volume of blood ejected by the heart travels back to the heart through the venous system to be pumped to the lungs and then oxygenated again. By studying these events through image analysis you can see how there are changes directly related to the cardiac events described. The parameter that can be extracted from the color changes is the HR. There are some methods for extraction such as separation into the three RGB channels and subsequent analysis of independent components (ICA) developed by (Poh, McDuff, and Picard 2010). The area they selected for the acquisition of the image was the face and as a reference the pulse was taken in the finger with a blood volume sensor.

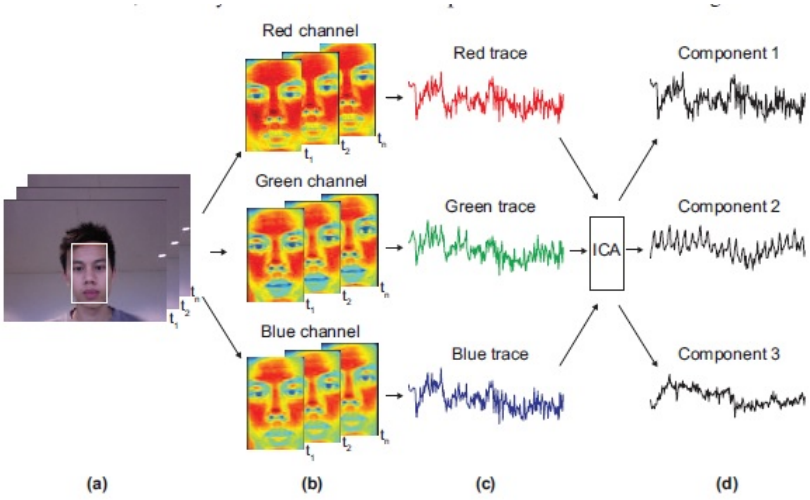

Figure 1.4: Cardiac pulse extraction using ICA method (Poh, McDuff, and Picard 2010).

Another method for extraction is used in (H.-Y. Wu et al. 2012). In this case there is some difference, as it also focuses on the visualization of changes. Thus, a decomposition is done in different spatial frequency bands, the same temporal filtering for each of the bands and an amplification. Finally, they generate a video signal in which you can see the color changes in a magnified way.

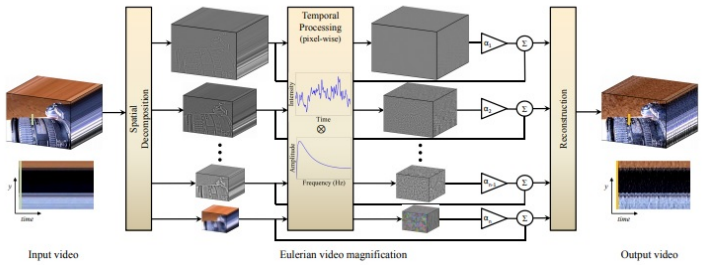

Figure 1.5: Eulerian Video Magnification algorithm (H.-Y. Wu et al. 2012).

Among all the techniques exposed in this section, the least intrusive for the patient is the extraction of features from image analysis. This is due to the fact that the patient and the device are far away so that there is no physical contact. The present work has focused on this technique and its objectives are found in the following section. The system to be designed in this work must consist of a pair of cameras located side by side. Using only one of the cameras is intended to extract information related to HR by studying the color changes in the image. The purpose of the pair of cameras is to determine the depth information to extract the breathing signal.

1.2 Objectives of the work

Objective 1

To propose a non-intrusive neonatal monitoring system with which HR and BR can be measured. The system should be inmune to movement artifacts and noise.

Objective 2

To design and build a mechanical structure as an initial prototype for image acquisition in the hospital. The structure must be adapted to both the cradle and the incubator in the *Neonatal Intensive Care Unit* of the *Hospital General de Valencia*.

Objective 3

To propose and develop calibration experiments for the cameras to be used in order to ensure a quality signal free of unwanted components.

Objective 4

To define a protocol of action adapted to the conditions in the hospital and carry out the acquisition of data based on it. Process the data and validate the results.

1.3 General context

The development of the present work has been carried out in the framework of a *VLC-Bioclinic* project, entitled *NEO9TEC. Diagnóstico precoz de la sepsis neonatal mediante la monitorización de la variabilidad cardiac* whose principal researchers where Dr. Empar Lurbe Ferrer and Dr. Javier Calpe Maravilla, where I received a pre-doctoral researcher position at the *Universitat de València*. This project was a joint venture between the Image *Processing Laboratory (IPL)* of the *Universitat de València* and the *Neonatology Intensive Care Unit* of the *Hospital General de València*.The project was supported by *Analog Devices, Inc.* Most of my time was spent between the *IPL* and *ADI*.

Chapter 2

Methods and materials

2.1 System description

The designed system consists in two aligned video cameras separated by a distance d, which is calculated depending on the distance to the object and the required depth resolution (Vision 2019). The two video cameras are supported by a mechanical structure that allows a vertical camera orientation as well as horizontal orientation and it is separated in two different modules; that allows the acquisition of images in both hospital and laboratory and provides absolute stability indoors and reasonable stability outdoors. This is key as some experiments and tests with natural light have been carried out outdoors. The fact of being outdoors limits the tests due to wind or other meteorological phenomena but provides natural light conditions. The two module design allows the system to work in two different applications and places: in a crib and in a incubator (see figure 2.1).

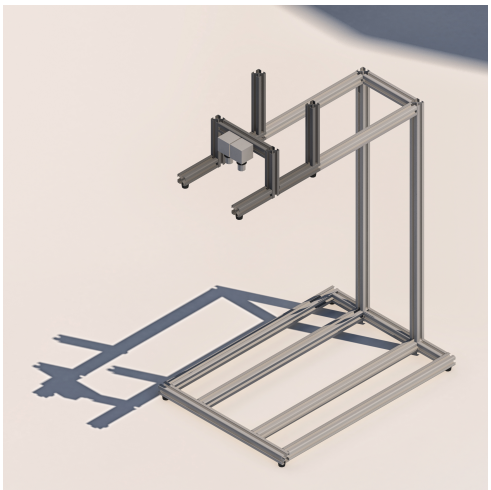

Figure 2.1: Two modules structure: module 1 (dark grey) and module 2 (light grey)

Figure 2.2 shows the parallel camera axis configuration where f is the focal distance (distance between the optical center of the lens and the sensor that detects the light information), d is the the distance between the two camera axis, P is the pixel in the depth scene, PL and PR are the projected pixels in the left and right camera lens respectively,xL and xR are the distances between the projected pixels and the left and right camera axis respectively, yL and yR are the two camera axis and yT is the central axis. Both the specifications of the video cameras and the prototype of the mechanical support system, where the devices are located, are described in section 2.2. The distance between cameras was calculated from the baseline distance calculator provided by Nerian (Vision 2019). For the calculation, the minimum depth at *0.35 m*, the focal length at *8 mm*, the size of the sensor whose diagonal was *7.81 mm* and the resolution of the sensor at *1280x1024 pixels* were set as parameters. The calculated baseline distance was *5.3 cm*.

The monitoring system extracts two vital signs; on the one hand, the BR monitoring is estimated from a depth map information with a *python* application, described in the following section. In this part, both cameras are used simultaneously and it is the reason of making a stereo-pair system. On the other hand, the HR monitoring is estimated from the change in the color.

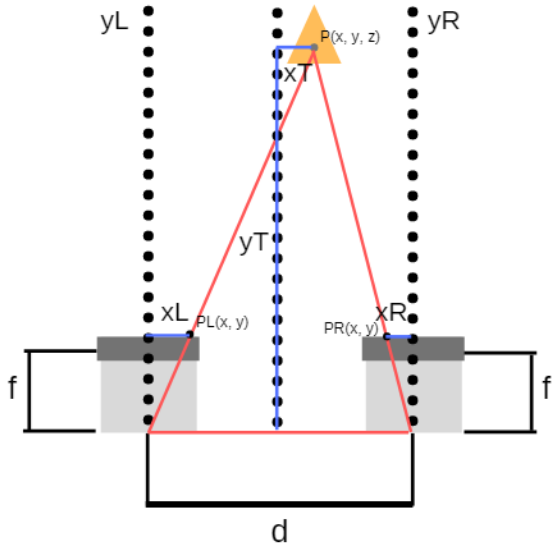

Figure 2.2: Stereo pair system and a single point in the space.

2.2 Hardware

2.2.1 Stereo video-cameras system

BASLER acA1300 - 200 uc

The video camera used in this project is the *acA1300-200uc* model provided by *BASLER*. The system specifications are presented in table 2.1 and the camera specifications are itemized in table 2.2. As can be seen, this camera fulfills the specifications.

Resolution (HxV in pixels)	1280 x 1024
Frame Rate	200
Bit Depth (bits)	8
Exposure Time	Programmable
Synchronization	SW/HW trigger
Working Distance Range	(0.4 - 0.6) m

Table 2.1: Required camera specifications.

Shutter	Global
Sensor Type	CMOS
Sensor Size (mm)	6.1 x 4.9
Resolution (HxV in pixels)	1280 x 1024
Frame Rate	203
Bit Depth (bits)	10
Interface	USB 3.0
Exposure Control	Programmable
Synchronization	SW/HW trigger
Housing Temperature (°C)	0-50
Minimum Working Distance	0.1 m

Table 2.2: Camera specifications (BASLER n.d.).

As far as the economic cost, the economic limit is set at 3000 €. Therefore, the economic cost of the materials of the system should not exceed this amount. In chapter 5 the information related to the economic costs of both hardware and other concepts is detailed.

Figure 2.3: The selected video camera: *BASLER acA1300 - 200 uc* (BASLER n.d.)

Regarding the camera sensor, this device includes a CMOS sensor. A CMOS sensor consists in an array of pixels organized into row and columns and its operation is based on each of the pixels generating a current that is proportional to the amount of light it receives; this determines the information in order to build the image. The size of the sensor is *6.1 mm x 4.9 mm* providing a resolution of *1280 x 1024 pixels*. The pixel bit depth is 10 bits and it is enough to the work application. As far as the acquisition image method, the camera works with global shutter; it means that, all light-sensitive pixels offer a current value simultaneously.

As far as the acquisition frequency, this video camera has been chosen because it can reach 200 frames per second (*fps*). In order to justify this value, only the HR value has been taken into account because its values are always higher than the BR ones and, therefore, more restrictive and

demanding. Discussing with the doctors we concluded that a 3 bpm resolution beat value for the application of this monitoring system was acceptable. As discussed in the previous sections, the normal or non-pathological HR range of newborns is approximately 70 to 180 beats per minute, unlike adults whose range is 50 to 100 beats per minute. Therefore, the maximum HR value is set at the most restrictive value, i.e. 180 bpm. The calculation of the minimum acquisition frequency so that the system can detect changes of 3 bpm is given by the following equations:

$$\left.\begin{aligned} HR_1 &= \frac{60}{180} \\ HR_2 &= \frac{60}{183} \end{aligned}\right\} \tag{2.1}$$

$$\Delta HR = HR_1 - HR_2 \tag{2.2}$$

$$f = \frac{1}{\Delta HR} \tag{2.3}$$

Where HR_1 is a HR value in seconds, HR_2 is the next HR value in seconds, f is the fixed acquisition frequency value and ΔHR is the value of the temporal resolution. Then, with a 183 bpm as maximum HR value and replacing it in Equation 2.2, the acquisition frequency is obtained using Equation 2.3:

$$\Delta HR = \frac{60}{180} - \frac{60}{183} = 5.464\ ms$$

$$f = \frac{1}{\Delta HR} = \frac{1}{0.00546} = 183\ frames\ per\ second$$

As it can be observed, to achieve a 3 bpm resolution beat at least a acquisition frequency of 183 fps is needed. In order to give a bit of margin for higher HR values a suitable value is 200 fps. Moreover, exploring other options with video cameras with higher acquisition frequency we realized that the price of them exceeded our project.

BASLER Lens C125-0818-5M

Regarding the video camera lens, a Basler Lens C125-0818-5M has been selected because it meets all requirements. One of the most important is the distance at which the video is recorded. Both in incubator and in cradle the distance can vary a few centimeters, so it is necessary to review the size of them and, above all, take measurements of the material that can be found in the place where the acquisition of images is done. Thus, the approximate height of an incubator is between 45 and 60 cm. On the other hand, the cradle has no height restriction since it is not a closed structure like the incubator; therefore, the height is imposed by the hospital incubators. In order to address the problem of height, a mechanical support that eliminate this barrier has been designed and mounted (described in the following section) and, in addition, the camera lens has a 100 mm minimum working distance. The working distance is the distance between the subject and the lens surface.

Figure 2.4: The selected lens *BASLER Lens C125-0818-5M*

Mechanical support for the cameras

As mentioned above, the mechanical structure consists of two different modules that can be joined together to create a single structure (the drawings of the designed structure can be found in Annexes). This is done with the aim of adapting the prototype to both scenarios: cradle and incubator. Module 1 is designed for incubator and can adopt two different positions depending on the need of the moment. This module is where the cameras are located and, for the initial tests, it is placed on top of the incubator, leaving the newborn in a position perpendicular to the direction of the cameras axes. The second module is designed for the other scenario: the cradle. The support that serves as the base is placed under the cradle being fixed to the bars of the trolley on which the cradle is located. The materials used to build both modules were purchased from (Motedis n.d.). The total cost of the materials of mechanical structure is detailed in chapter 5.

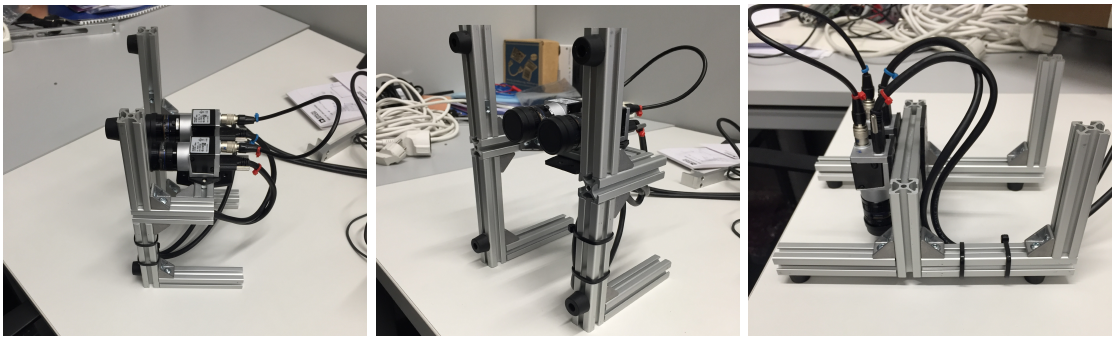

(a) Side view in vertical position **(b)** Front view in vertical position **(c)** Side view in horizontal position

Figure 2.5: Views of the module 1 of the mechanical structure support.

For the design and construction of the prototype, physical measurements were taken of both the cradle and the incubator. What we measured was:

- Width of the crib/incubator and width of the support structure that transports the crib.
- Length of the crib/incubator and length of the support structure that transports the crib.
- Diameter of the support structure bars.

Figure 2.7 shows the incubators of the *Neonatal Intensive Care Unit (Neonatal ICU)*. The module 1 is placed on top of the incubators. Figure 2.8 shows the cradles of the *Neonatal ICU*.

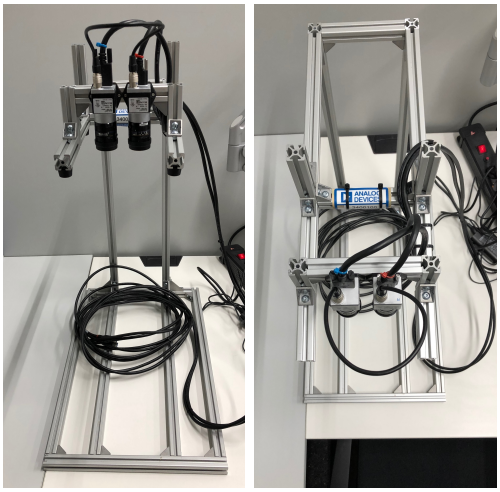

(a) Front view. **(b)** Top view.

Figure 2.6: Views of the module 2 of the mechanical structure support.

Here, both modules are used by attaching themselves to the bars of the trolley on which the cradle rests.

(a) Side view in vertical position **(b)** Front view in vertical position **(c)** Side view in horizontal position

Figure 2.7: Views of the incubators. The module 1 of the mechanical structure is on of the incubator.

(a) Side view in vertical position **(b)** Front view in vertical position

Figure 2.8: Views of the cradles.

2.2.2 Acquisition software: Pylon Viewer and Pypylon

The image acquisition software is *Pylon Viewer*, developed by the camera manufacturer BASLER. This software allows configuring the parameters of the cameras and programming the image acquisition processes. In addition, the manufacturer provides a *Python* library with which you can program in python the configuration of the cameras and make use of them. *Pylon Viewer* has been used to configure the synchronization of the cameras so that one of the cameras is the master camera and the other is the slave camera. In this way, both cameras can be activated simultaneously for the image acquisition process for the stereoscopic application. Table 2.3 details the configuration of both the master and slave cameras.

PARAMETER	CAMERA 1 (**Master**)		CAMERA 2 (**Slave**)	
Acquisition Control	**Enable Acquisition Frame Rate**	Enabled	**Trigger Mode**	On
	Acquisition Frame Rate	Adjust to value	**Trigger Source**	Line 4
	-	-	**Trigger Activation**	Falling Edge
Digital I/O Control	**Line Selector**	Line 3	-	-
	Line Mode	Output	-	-
	Line Source	Exposure Active	-	-
Image Quality Control	**Balance White Ratio**	Once	**Balance White Ratio**	Once

Table 2.3: Settings for the acquisition process of stereo images and cameras syncronization.

2.2.3 Processing software: Python

Once video acquisitions have been made, the data must be processed. The data processing tasks were performed with open source programming language *Python*.

2.3 Camera calibration

Since we are taking accurate quantitative measurements based on the image, we need extensive calibration in order to account for all the potential distortion in the acquired images. It is essential to perform some experiments to know the response the camera is delivering under certain conditions. Those experiments require the use of an integrating sphere. These ones and the conditions under which the experiments have been developed are described in the sections below.

2.3.1 Integrating sphere experiment

The integrating sphere

The integrating sphere is a device that can provide a uniform illumination with a reasonable accuracy. The used sphere model for experiment has been the *US-080-SF* by *Labsphere.*The main characteristics of the US-080-SF model is described below. Regarding the dimensions of the sphere, it has a 8" diameter and two main output ports of 1 and 2" diameter. The 2" diameter is related to the output port sphere, where the camera is placed and the 1" diameter one is for the light source. As far as the materials, the integrating sphere is coated with *Spectraflect* and it's available with 80% and 98% reflectances. The *Spectraflect* material has high reflectance, it is highly lambertian, non-toxic and it provides optical stability [*Labsphere n.d.(b)*].

This device has been used in order to determine and quantify the possible level and type of noise the camera is introducing into the images. We propose two kind of studies; on the one hand, a linearity study to understand the response the camera is giving and, in the other hand, an image spatial homogeneity study to understand the distribution of the possible noise and interference in the acquired data.

The light source type used in this experiment is an *External Halogen Light Source (EHLS)* and it provides an adjustable radiation level. The model of the light source is the *EHLS-100-75R* and it is manufactured by *Labsphere* [*Labsphere n.d.(a)*].

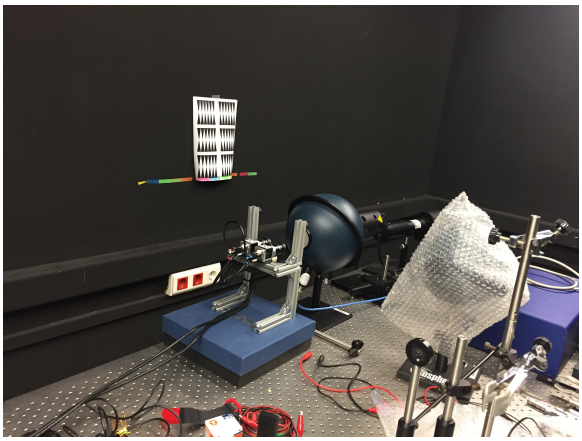

Figure 2.9: Integrating sphere experiments room.

Linearity study

The linearity study is described in this section. This study aims to assess whether the video cameras behaviour is linear or not. To do that, we analyze the following variables: integrating time, light source current, camera temperature and grey level with respect to the received intensity level signal. Integrating time is the time period in which the shutter of the image sensor of the camera is open and it is limited by the acquisition frequency. Therefore, the longer the integration time, more light it's captured and there is a higher saturation probability; the integrating time values set is *(5, 3.125, 2.5, 1.563, 1.25) ms*. The light source current value is the current that the generator is applying to the lamp light and its values set is *(0.005, 0.008, 0.01, 0.016, 0.02) mA*. The camera temperature values range usually is from ambient temperature *(25 - 30) °C* at the initial power on moment to *70 °C* as the maximum housing temperature established by *UL 60950-1* [*Basler n.d.*]. The grey level values range is a digital count from 0 to 255 in *full-gray scale MONO 8* format, where 0 is darkest value in the grey scale and 255 is the brightest value in the same scale.

The first part of study is the temperature analysis; it can determine which is the camera temperature during the acquisition and, also, it can inform the technician about a possible needed warm-up time until the operating temperature is reached. The used software to program the temperature measurements protocol is *Python* with the *pypylon* module specifically created for *BASLER* cameras models. The measurements test consists of temperature and intensity signal (gray level) data acquisition once a second (sampling frequency: 1 Hz) over the course of 15 minutes. In order to see whether a low temperature at the first few seconds has relevant effects

or not, the gray level captured by the sensor has been evaluated over the full time of test. The gray level is obtained by calculating the average pixel value enclosed in a region whose size is defined by two programmed parameters: width and height. Width defines the amount of pixels in the horizontal axis and height defines the amount of pixels in the vertical axis. The temperature values and gray level values as time functions are plotted in the results with the aim of visualizing the temperature curve and the gray level variability to check if it's affected by the temperature. In table 2.4 the characteristics of the acquired video for temperature analysis are shown.

ROI Width (px)	**ROI Height** (px)	**Frame Rate** (fps)	**Duration** (min)	**#Frames**
528	414	1	15	900

Table 2.4: Video data for temperature analysis.

The second part of the study is an integrating time and light source current analysis. The results of this part can establish the linear response of the camera. The measured variables are the integrating time *(ms)*, the light source current *(mA)* and the intensity level, in each channel, calculated as the mean value of all the pixels. (Camera output channels described in the hardware description section). To reduce the amount of data and to be able to select different areas of the full acquired image, a *Region Of Interest (ROI)* has been chosen. The first integrating time value of the experiment is established trying to match with the hospital lighting conditions, where the final video acquisition takes place. The video data acquisition of this part of the experiment has been done by taking data with different integrating times and light source currents values, beginning with the mentioned first integrating time value and progressively reducing it. At the same time, the light source current values have been changed inversely proportional to the integrating time values. In table 2.5 the characteristics of the five acquired videos for this part of the linearity study are shown. The color intensity level variable as a function of integrating time and as a function of light source current is plotted in the results section.

Video n°	**IT** (ms)	**LC** (mA)	**ROI W** (px)	**ROI H** (px)	**FR** (fps)	**Duration** (s)	**#Frames**
1	5	0.005					
2	3.125	0.008					
3	2.5	0.01	110	107	200	5	1003
4	1.563	0.016					
5	1.25	0.02					

Table 2.5: Video data for integrating time and light source current analysis. **ROI W**: Width of the ROI. **ROI H**: Height of the ROI. **FR**: Frame Rate.

The results and conclusions of the study are included in the *Results* section.

Homogeneity study

This study has been done with the aim of visualizing the possible noise, introduced by the camera and of the acquired image, quantifying its level, understanding how the noise is described in the image and seeing whether there is some noise pattern that is produced continuously at acquisition time. The homogeneity analysis has been performed for the different integrating time and light source current values, described previously in the linearity study section, and storing the color intensity level in each RGB channel. The way to proceed in this analysis is similar to the linearity study, but with some differences; this time a standard deviation values matrix, an average pixel values matrix, a histogram and the standard deviation function over the time are generated for each channel. On the one hand, the first one is done by creating an array of the pixel value at same location over the time for each pixel of the *(ROI)* and calculating its standard deviation. This is plotted by a color map graphic with the objective of describing visually the noise. The average pixel values matrix is generated in order to be able to see the possible non-uniformity in the image. To do this, the mean values matrix of the whole matrices of the acquired data has been calculated and plotted as a color map as well. On the other hand, the histogram is obtained to see the distribution of the mean pixel values over the time and the standard deviation function is calculated for each frame (pixel values matrix). Moreover, it has been considered necessary the assessment of a single pixel value over the time due to the interest of checking the randomness of its noise. In order to get the optimal *(ROI)*, a standard deviation curve has been calculated choosing different ROI size values progressively. The results and conclusions of the study are included in the *Results* section.

2.4 Video acquisition protocol

For the image acquisition process we elaborate a test protocol to be followed, once we're in the hospital, in order to streamline processes and minimize interference with hospital activity. It should be noted that the tests are performed in the *Neonatal ICU* of the *Hospital General de Valencia* and some of the neonates are in a critical state due to a premature birth or some pathology they suffer. In addition, there is the stress of parents, doctors and nurses who contribute to a demanding and sensitive work environment. The protocol is divided into 2 phases. The first one is the hardware and software configuration of the equipment. It involves these steps:

(i) We place and fix the cameras in the crib or in the incubator, depending on the application.

(ii) We perform a manual focusing to the desired position in order to do the stereo calibration process afterwards.

(iii) We set the following camera parameters at reasonable values: exposure/integration time, gain and white balance (once).

(iv) We generate a calibration file to guarantee depth accuracy using a predefined checkboard pattern in the incubator or crib without a neonate.

(v) We acquire video data with the software *Pylon Viewer*.

The second phase of the protocol involves the calibration of the stereo pair in order to get accurate depth measurements. It corresponds to the use of *Pylon Viewer* with which we do

the camera configuration and image acquisition according to the application. The two types of measurements, as explained in previous sections, are HR measurement and BR measurement so the first one requires a different software configuration from the second one. As for HR:

(i) Power on only one video camera.

(ii) Select a region of interest to decrease the amount of acquired data.

(iii) Frame rate: 200 fps.

(iv) Exposure time < 4 ms.

(v) Set a high analog gain depending on the light conditions.

As for BR:

(i) Power on both video cameras.

(ii) Do not establish a region of interest.

(iii) Frame rate: 30 fps.

(iv) Exposure time: < 10 ms.

(v) Set the analog gain between 0 or 3 dB.

2.5 Color techniques for HR estimation

RGB is a color space, or also called a chromatic model, in which the primary colors are red, green, and blue; these are the colors from which most imaging devices construct images. All the different colors that compound the images we visualize are created by combining these three colors additively; this is known as additive color synthesis. As its name implies, the combination to obtain other colors is done by adding the value of each red, green and blue component, represented on a given scale. The camera used in the system has an 8-bit RGB format, i.e, it allows 255 different values for each color. As examples, if the three main components have a value of 0, the resulting color is completely black and if they have the maximum value, the resulting color is completely white (Nishad and Chezian 2013).

The technique used in this work for the extraction of the HR is the analysis of color changes in an image in each of the three channels: R, G and B. The camera sensor used in the prototype has a Bayer filter, also known as Bayer mosaic (figure 2.10). It is a matrix of alternating filters, so each component of the matrix is a color filter. The matrix components determines the number of pixels and, therefore, each pixel shows only one component and only one color. One of the most known filters is Bayer filter, which defines in each group of 4 pixels the following configuration: 2 green pixels, 1 red pixel and 1 blue pixel. This allows to obtain double the resolution in the green component of the resulting image than in the red and blue components. This configuration is justified on the grounds that the human eye is more sensitive to wavelengths in the mid-area of the visible spectrum; the wavelength range of the visible spectrum is from 400 nm to approximately 750 nm. The values of the green component range from 500 nm to 570 nm, i.e. in the mid-area of the visible spectrum (Maschal Jr et al. 2010).

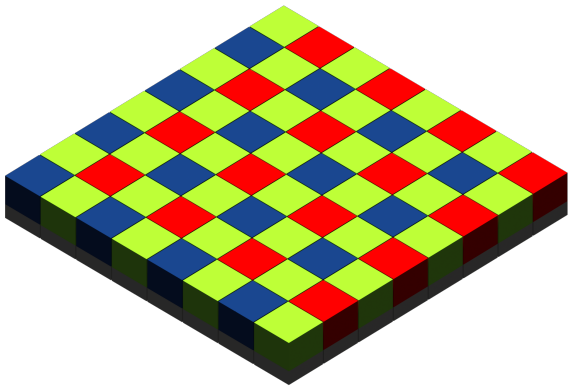

Figure 2.10: CCD sensor with the Bayer pattern mosaic.

This technique is based on the idea that there are color differences in the skin depending on the cardiac event in which we are. During systole, the heart pumps the blood and the circulatory system is responsible for distributing it, so that the blood reaches the tissues traveling through the smallest arteries and this is reflected in the color of our skin; it is then when the light reflected and detected by the light sensors is greater. By contrast, during diastole the heart relaxes and the filling of the circulatory blood begins; it is then when the light reflected and detected by the sensors is lower. This is due to the behaviour of haemoglobin: the oxygen-carrying protein. During systole, hemoglobin is oxygenated, and during diastole, deoxygenated (reduced). It is

known that, in red light (660 nm), oxygenated hemooglobin has a lower extinction coefficient than reduced hemooglobin (Jubran 2015). In figure 2.11 the extinction coefficient of four kind of hemoglobin is plotted as a function of wavelength. Although this concept is more focused on pulsioximetry applications, it can explain why the sensors of the cameras used in this work receive more light at the time of blood pumping.

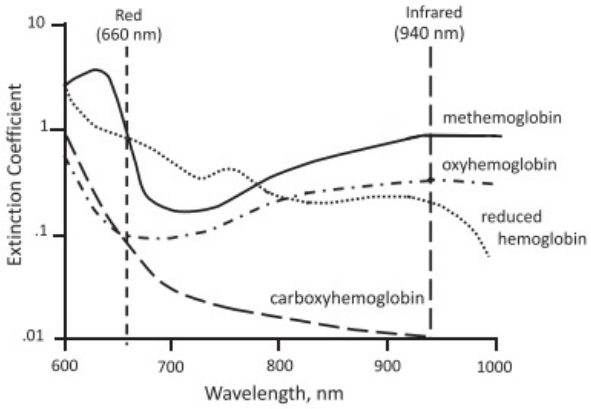

Figure 2.11: Light absorbance spectra of four types of hemoglobin (Jubran 2015).

Light absorption is maximum when there is no reflectance. That is to say, when all the energy of the light is trapped in the body on which it falls. This suggests that skin pigmentation in humans is very important to explain the reflectance of light from the body surface. As demonstrated (Norvang et al. 1997), in fairer skins the reflectance is higher and in darker skins the reflectance is lower. In figure 2.12 the differences of reflectance among different kind of skins are shown.

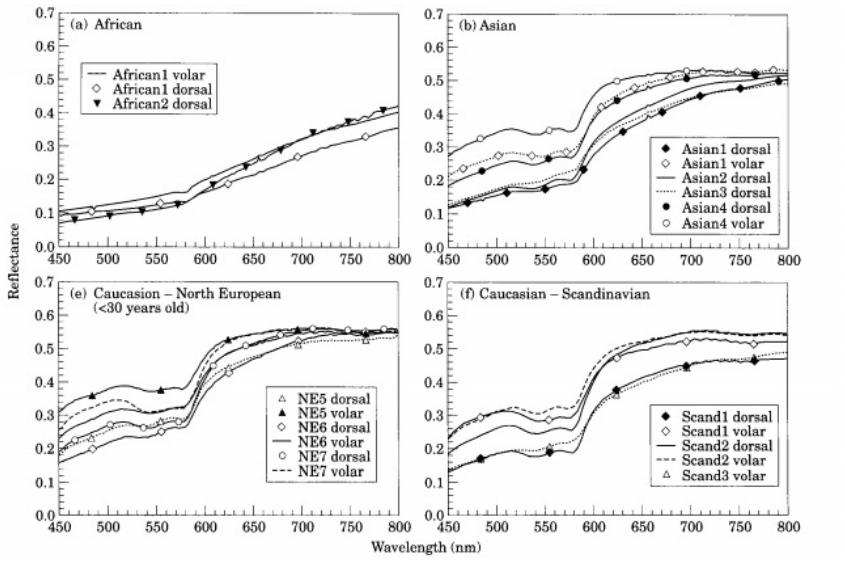

Figure 2.12: Light reflectance in different skin sites classified according to the human race (Norvang et al. 1997).

2.5.1 ROI location

As discussed above, more light absorption on the skin should change with the cardiac cycle, identifying when the wave pulse with oxygenated blood gets to a certain point of the circulatory system. It seems logical to think that choosing a *ROI* of a certain size and locating it as close to the heart as possible would give you highly contrasted signal that would simplify the identification of the color change during blood circulation. But to corroborate this, some evidence is needed. Therefore, the first step was the selection of the *ROI* location. This procedure was done by trial and error, choosing a body area and checking the results of the integrated reflectance signal measured there. The body areas chosen were the left and right chest, sternum and abdomen. The second step was the image processing. It was done offline. In order to do the second step, an application was developed using the *Python* programming language in the *Pycharm* environment; it allows to open and play the video, as well as to display the signal of the RGB channels (not simultaneously). In figure 2.13 the described application is shown. In parallel, another application has been developed to process the three *RGB* acquired signals. The purpose of this is to be able to visualize the evolution of each channel at each frame. With the same philosophy as in calibration experiments section, it is important to reduce the amount of data to be processed so as not to saturate and reduce the computational cost of the process and, thus, avoid problems. In consequence, it is important to find a reasonable balance between the size of the data and the results obtained. The video to be processed is a four-dimensional matrix. The first two dimensions are the width and height of the image represented in number of pixels, the third one is each of the three *RGB* channels and the fourth one is the number of images that the video sequence has. To evaluate the change in color for the image over time, a set of values with each *RGB* average value ($X_R(l)$, $X_G(l)$ and $X_B(l)$) of l frames has been calculated as follows:

$$\mathrm{R} = \begin{pmatrix} r_{11} & r_{12} & r_{13} & \dots & r_{1j} \\ r_{21} & r_{22} & r_{23} & \dots & r_{2j} \\ \dots & \dots & \dots & \dots & \dots \\ r_{i1} & r_{i2} & r_{i3} & \dots & r_{ij} \end{pmatrix}; \mathrm{G} = \begin{pmatrix} g_{11} & g_{12} & g_{13} & \dots & g_{1j} \\ g_{21} & g_{22} & g_{23} & \dots & g_{2j} \\ \dots & \dots & \dots & \dots & \dots \\ g_{i1} & g_{i2} & g_{i3} & \dots & g_{ij} \end{pmatrix}; \mathrm{B} = \begin{pmatrix} b_{11} & b_{12} & b_{13} & \dots & b_{1j} \\ b_{21} & b_{22} & b_{23} & \dots & b_{2j} \\ \dots & \dots & \dots & \dots & \dots \\ b_{i1} & b_{i2} & b_{i3} & \dots & b_{ij} \end{pmatrix} \quad (2.4)$$

$$x_R(l) = \frac{1}{n}\frac{1}{k}\sum_{i=1}^{n}\sum_{j=1}^{k} x_{Rij}(l) \quad (2.5)$$

$$x_G(l) = \frac{1}{n}\frac{1}{k}\sum_{i=1}^{n}\sum_{j=1}^{k} x_{Gij}(l) \quad (2.6)$$

$$x_B(l) = \frac{1}{n}\frac{1}{k}\sum_{i=1}^{n}\sum_{j=1}^{k} x_{Bij}(l) \quad (2.7)$$

where n is the number of rows in each frame defined by the parameter *height* of the *ROI*, k is the number of columns in each frame defined by the parameter *width* of the *ROI*, and $x_{Rij}(l)$, $x_{Gij}(l)$ and $x_{Bij}(l)$ are each pixel value of each red, blue and green frame of the video sequence.

Figure 2.13 shows the application developed for video visualization, signal processing and real-time processing visualization. In the left box we show all the parameters that can be modified for both video display and processing. On the right side there are two panels: on the top one the video is displayed and on the bottom one, one of the 3 channels is displayed. The steps to use the application are simple: first, we click on "load video" to upload video. It is optional to choose the "log on" box. If this box is selected, it will generate a *.csv* file in which both the descriptive data of the video and the signals of the 3 RGB channels are stored. The purpose of this is to be able to do a post processing of the signal since the processing that can be done in real time is limited to the options that will be described next. Secondly, the parameters below can be used to configure the *ROI*. Thirdly, we click on "Play" button for the video to start playing. Real-time processing is limited to choosing the cutoff frequency value of the high pass and low pass filters at the end of *Parameters* block. In addition, in the display mode you can choose which channel you want to show and whether or not to apply the filter.

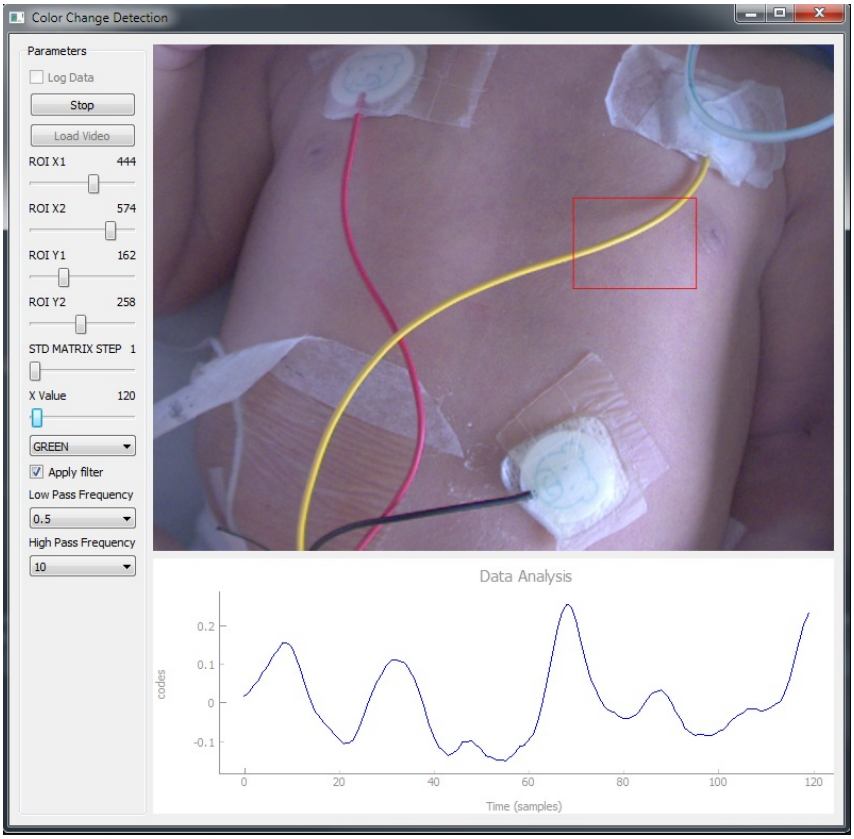

Figure 2.13: Designed application in order to visualize the acquired signal in the ROI while the video is playing and processing.

As mentioned above, the procedure for deciding the best *ROI* zone has been based on trial and error. To do so, several acquisitions have been made in the specified areas. In table 2.6, the main characteristics of each video are shown. The size of the *ROI* for the *ROI* location assessment is the maximum size that is not affected by other objects that are on the neonate's body.

Video n°	**Body Area**	**ROI Width** (pixels)	**ROI Height** (pixels)	**Frame Rate** (fps)
1	Left chest	80	80	200
2	Right chest			
3	Sternum			
4	Abdomen			

Table 2.6: Video data for finding the best ROI location.

Once the four locations were decided, we proceeded to obtain data from the different ROI locations. The quality of the signal obtained for the different locations was evaluated; the parameters that were taken into account to determine the quality of the signal were the amplitude of the signal in *LSBs*, value of the highest peak in the frequency spectrum in dB and in *Hz*, value of the second highest peak in *dB* and in *Hz*, value of the difference between the highest peak and the second highest peak in *dB*, and the *signal-to-noise ratio*. All the measurements were obtained for the same time value. The difference between the highest peak in *dB* and the second highest peak in *dB* is defined in the Equation 2.8. The *signal-to-noise ratio* is defined by the difference between the highest peak in *dB* and the *Noise Floor* value in *dB* (Equation 2.9).

$$\Delta MPP = MPP1 - MPP2 \tag{2.8}$$

$$SNR = MPP1 - NFP \tag{2.9}$$

In the file generated with the application described above, all the values calculated using Equation 2.5, Equation 2.6 and Equation 2.7 have been stored; The procedures were repeated and applied to the acquired videos obtaining a very similar pattern of results in all the videos; in chapter 3 the results of one video analysis are elaborated.

The four *ROIs* for the location assessment are shown in figure 2.14. In order not to interfere with or contaminate the signal obtained, the regions have been chosen in such a way that no object or shadow is present within each region. As shown in figure 2.14, the neonate has several wires connected to measure the *ECG* signal, which should be excluded from the *ROI*.

In summary, the procedure for the assessment of the *ROI* location was the same for each acquired video and it was as follows: first, the *ROI* was placed; secondly, the generated data in the *ROI* was processed. Thirdly, some characteristics were extracted and, finally, the best *ROI* location was selected. Note that this procedure was replicated for each acquired video with similar results.

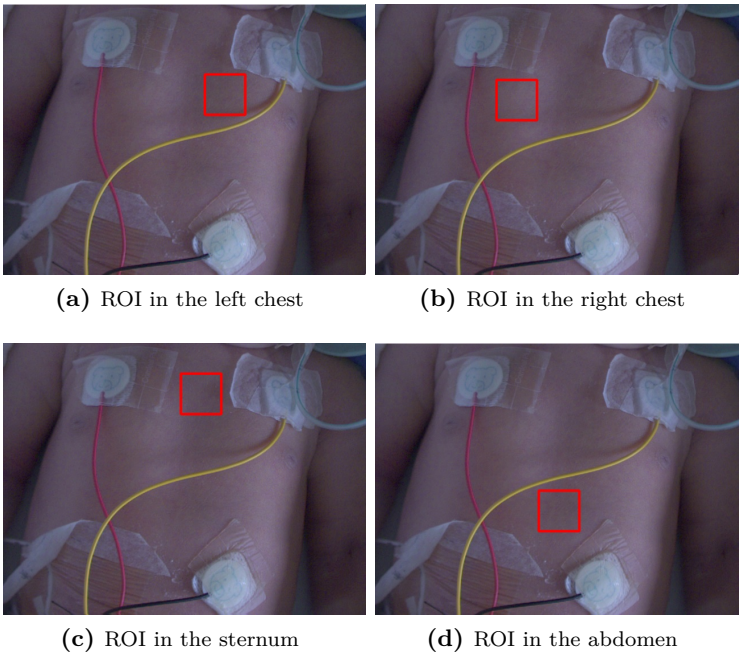

(a) ROI in the left chest **(b)** ROI in the right chest

(c) ROI in the sternum **(d)** ROI in the abdomen

Figure 2.14: The four ROI locations.

2.5.2 ROI Size

The procedure for choose the size of the *ROI* followed a very similar methodology to that used in the justification of the *ROI* location. Here, there is a trade off with respect to the ROI: a bigger ROI reduces pixel variation but too big ROi will smooth the response. Then, a ROI size value must be achieved that is adequate enough to capture the necessary variations and at the same time be robust against elements that may be introduced into the ROI. In this case, an area was chosen where a good signal level was observed: the area of the left chest, very close to the location of the heart. This area, as detailed in the results section, is where the best results were obtained. Six different sizes were evaluated: *140x140*, *110x110*, *80x80*, *60x60*, *40x40* and *20x20* (in pixels). The way in which the *ROI* was delimited was fixing its center. In other words, all the different *ROI* evaluated shared a geometric center.

Once the location was decided, we proceeded to obtain HR signals for different size values. By means of trial and error, the quality of the signal obtained for the different sizes was evaluated; the parameters that were taken into account to determine the quality of the signal were amplitude of the signal in *LSBs*, value of the highest peak in the frequency spectrum in *dB* and in *Hz*, value of the second highest peak in *dB* and in *Hz*, value of the difference between these two peaks in *dB*, the signal-to-noise ratio and the mean value of the standard deviation matrix of the *ROI*. The way to calculate the standard deviation matrix is defined at subsection 2.3.1. The standard deviation captures the homogeneity of the image. The standard deviation establishes how close the value of one pixel is to the arithmetic mean of a samples set (in this case the set of samples is made up of all the values acquired by the same pixel during the time the signal lasts). In calibration experiments section, the homogeneity of the image was evaluated in order to find noise patterns that could be affecting the image and having negative effects on the desired results. In this case, homogeneity was studied in order to find which region suffered the highest changes. If color

changes are well detected in a given region, this would mean that the standard deviation in that place has a higher value than the rest of the regions. If we cross-check the standard deviation data obtained with the rest of the parameters studied, we would be able to determine what is the optimal size of *ROI*. An additional parameter could be the standard deviation value of the standard deviation matrix; with this parameter we could analyze the variability of the *ROI*. But if we combine the mean standard deviation with the amplitude value of the signal we can estimate the intensity of the changes. All the measurements were obtained for the same time value. The results are detailed in chapter 3.

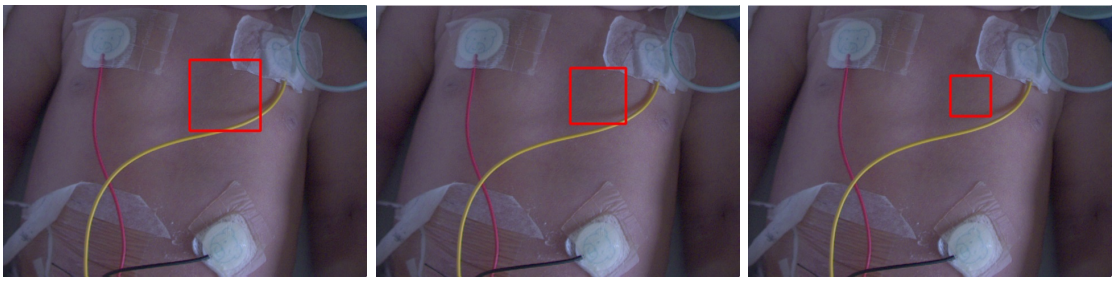

(a) ROI with size 140x140 pixels **(b)** ROI with size 110x110 pixels **(c)** ROI with size 80x80 pixels

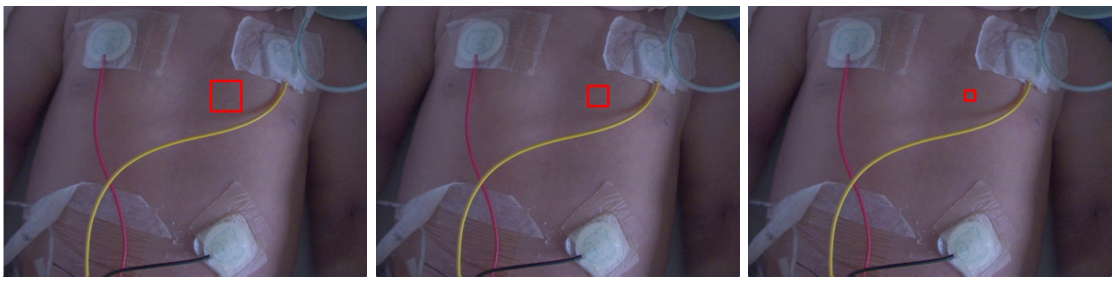

(d) ROI with size 60x60 pixels **(e)** ROI with size 40x40 pixels **(f)** ROI with size 20x20 pixels

Figure 2.15: The six ROI sizes.

Video n°	**Body Area**	**ROI Width** (pixels)	**ROI Height** (pixels)	**Frame Rate** (fps)
1	Left Chest	140	140	200
2		110	110	
3		80	80	
4		60	60	
5		40	40	
6		20	20	

Table 2.7: Video data for finding the best ROI size.

2.5.3 Signal Processing

The signal processing consists of three stages: elimination of very low frequency or *DC* component, a high pass filter and a low pass filter. In the sections below, each stage is described.

First stage

In the first stage the elimination of very low frequencies and the continuous component has been performed. To do this, the raw data previously obtained was subtracted from the average value of the string of values. We do this in order to guarantee the elimination of continuous component. Equation 2.10 and Equation 2.11 are arithmetic mean of a set of values and the signal to be processed without the average value, respectively:

$$\bar{x} = \frac{1}{n}\sum_{i=1}^{n} x_i \tag{2.10}$$

$$x(t) = x_i(t) - \bar{x} \tag{2.11}$$

where $x(t)$ is the processed signal, i is a range from 1 to n samples and $\bar{x}$ is the arithmetic mean definition.

Second stage

The second stage consists of a digital high pass filter that eliminates low frequencies as the movements of the neonates body. The choice of the cut-off frequency value is justified on the basis of the characterization of the signal to be obtained, in terms of frequency. Therefore, it was based on the HR ranges described in the literature and presented in chapter 1. The minimum frequency in neonates that is established under physiological conditions is 90 *bpms*; in other words: 1.5 *Hz*. This means that choosing a cut-off frequency of 1.5 *Hz* the bandwidth in the low-frequency zone would allow to have information of the signal of interest, as long as the neonate was in non pathological conditions. However, as long as the system has the ability to monitor lower than normal HR values, the cutoff frequency chosen for the high pass filter is 1.2 *Hz*. In this way, the system could detect HR values of up to 72 *bpms*. Regarding the type of filter, an *IIR* has been used. The choice is based on the fact that it can offer a good response without having to raise its order and that it has a good resolution especially at low frequencies. In addition, in the application of this work it is required that the phase delay and distortion be null or very low; therefore, the designed filter is applied bi-directionally. Equation 2.12 is the filter response expressed with the difference equation:

$$y(n) = \sum_{k=0}^{M} b_k \cdot x(n-k) - \sum_{k=1}^{N} a_k \cdot y(n-k) \tag{2.12}$$

where $y(n)$ is the filter output in a n time instant, b_k and a_k are the coefficients of the filter, $x(n-k)$ is the input signal to be filtered. The filter is developed with the *Python*-based echosystem *SciPy*. The used functions are: *butter* and *filtfilt*. On the one hand, with *butter* function the a and b coefficients were calculated. This function is based on *Butterworth* filter and needs a filter order,

a cutoff frequency and a last parameter to know if it is a high pass or low pass filter as an input argument. On the other hand, with *filtfilt* function the bi-directional filtering is performed. This function needs a and b coefficients previously calculated with the *butter* function and the signal to be filtered. Other input arguments in both functions can be included but they are optional.

Third stage

At this stage, the signal is processed by applying a low-pass type *IIR* filter. The choice of the cut-off frequency is justified in the same way as in the previous stage. Since the maximum HR in neonates is 165 *bpms* (2.75 *Hz*) and a margin is desired, the cutoff frequency has been set to 3.5 *Hz*. Moreover, the sampling rate was extracted from the acquisition frequency of the video to be processed. In figure 2.17 these three stages are shown with block diagrams and figure 2.16 shows both the raw signal and the processed signal.

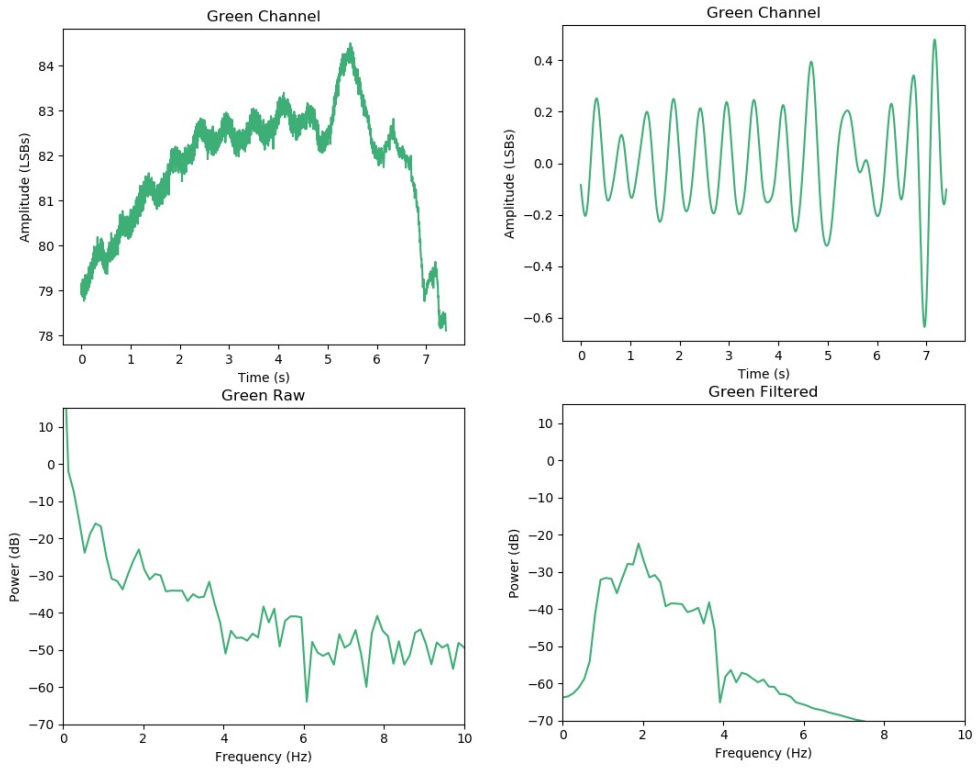

(a) HR estimation in the frequency spectrum **(b)** HR estimation in the time domain

Figure 2.16: Signal of the green channel calculated for the left chest ROI. In the top graphs the signal is shown in the time domain and in the bottom one the signal is shown in the frequency domain. **a)** No filtered signal. **b)** Filtered signal.

Figure 2.17: Block diagram of the 3 signal processing stages.

2.5.4 HR Estimation

In order to calculate the HR, we tried to use and implement in *Python* an algorithm designed by *Ronald M. Aarts* (Aarts 2004). This low-cost and low-complexity algorithm estimates the frequency and amplitude of sinusoid signals. The algorithm was chosen to display HR values since the signals obtained by the monitoring system have sinusoidal morphology. Alternatively, the estimation of the HR was made by studying the frequency spectrum. Thus, the highest peak of the signal sets the signal frequency value, which results in the neonate's HR. The *fft* function of the *SciPy* library has been used to calculate the discrete *Fourier* transform using the efficient *Fast Fourier Transform* algorithm (Cochran et al. 1967). Once the *Fourier* transform has been calculated, a function that finds the maximum value of a data vector has been used. In this case, the vector contains all the values obtained by the *fft* function. The *argmax* function has been used to extract this maximum value. As the vector generated in the Fourier transform calculation is given in *decibels*, the *argmax* function is also given in the same units.

We also explored the possibility of obtaining the HR time domain techniques using the *findpeaks* function of the *SciPy* library. The *findpeaks* function is able to find the value of the position where a local maximum is produced along the signal. Exploring the parameters with which the function can be adjusted to our needs, we have made use of the parameter that establishes the threshold for the peak is detectable, the prominence of the peaks and how many samples of minimum distance between peaks there should be. In figure 2.18, an example of the resulting HR estimation is shown. The signal corresponds to the green channel of a video acquired from an adult face and the *ROI* size was *80x80* pixels.

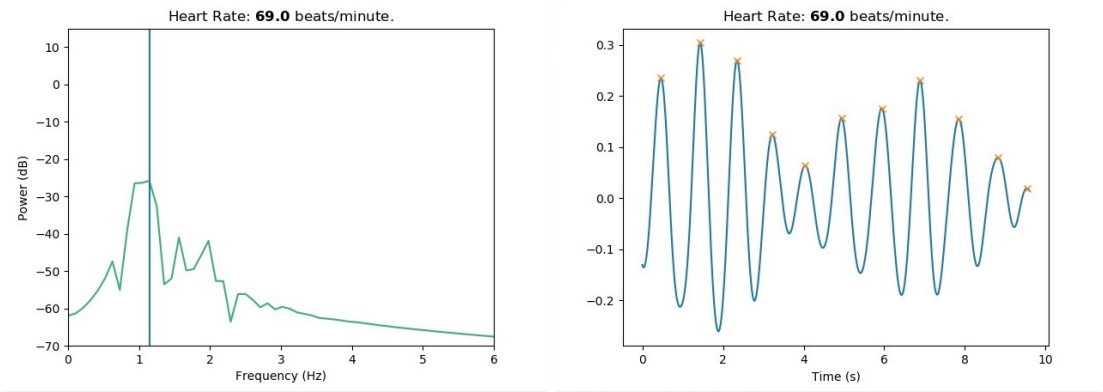

(a) **(b)**

Figure 2.18: a): Frequency spectrum of the HR signal and vertical line crossing the highest peak. b): HR signal in time domain with a detected peak mark.

Displaying HR values

One of the objectives of designing a monitoring system is to display a parameter in order to help the doctors in decision making during the diagnostic process. In order to do this, a strategy must be designed in such a way that the displayed value is adequate. Probably we would get a lot of variability by just showing the patient's last HR value. This could lead to unnecessary stress for both the patient and the doctors. Therefore, to achieve this goal, it has been proposed two ways to show the HR values. Both ways are based on the intervals function.

First strategy

As discussed in this section, the peaks that determine the HR were detected with *findpeaks* function. By obtaining these positions the value of the duration between two consecutive peaks can be calculated. This would add value to the system as it would allow studies of variability in the HR, key to determine possible pathologies directly related, or not, with the heart. The equation that defines the difference between the previous and subsequent peak in the time domain is described in Equation 2.13:

$$b_t = p_{t+1} - p_t \tag{2.13}$$

where p is the peak position signal and t is the number of samples that coincides with the number of peaks. So, in this way we obtain the mentioned intervals function of the heartbeat events. As an example, if we define a 500 samples window and the *findpeaks* function detects 10 peaks, the Equation 2.13 would have $t = 10$ samples. Therefore, this proposal is based on the calculation of found peaks interval average in a given window. That is to say, once the we get both the peak positions and the the difference between subsequent peaks in the acquired signal, we apply different weight value to each found interval. So, applying the mentioned weights to interval values we do a weighted average in which the most recent values acquire greater relevance without discarding history. The refresh rate of the system will be defined by the window size, previously established for the calculation of the peak positions. In Equation 2.14 we calculate the HR values that the system would display for the first proposed strategy. In Equation 2.15 and Equation 2.16 the way to calculate the weight value is shown:

$$x_n = \alpha \cdot x_{n-1} + \alpha \cdot \sum_{i=1}^{P} b_i \cdot (i+1) \tag{2.14}$$

$$\alpha + \alpha \cdot \sum_{i=1}^{P} (i+1) = 1 \tag{2.15}$$

$$\alpha = \frac{2}{P^2 + 3P + 2} \tag{2.16}$$

where α is the applied weight that remains constant, x_{n-1} is the previous HR value, P is the number of found peaks, b_i is the value of each founded peaks interval. Also, for the first data record that the system processes, Equation 2.14 needs the previous value to make the calculation.In order to solve it, only during the first data record at the time the monitoring is started, the system

will base the calculation of the first value only on the mean value of the record to show it. Its calculation is described in Equation 2.17:

$$x_0 = \frac{1}{P} \cdot \sum_{i=1}^{P} b_i \tag{2.17}$$

Second strategy

The second proposed strategy is also based on the calculation of the weighted average. The difference from the first proposed strategy is in the current one we add a window shift. Adding a window shift in the calculation of the HR value gives to the user of the device having more up-to-date information about the patient's situation. In addition, this time the refresh rate of the system is defined by the window shift in which the calculations are made and not by the size of the window as in the first proposed strategy. This implies a higher computational cost as the frequency of calculation increases. The equations that define this strategy is the same as the first proposed strategy (Equation 2.14 and Equation 2.15).

It should be remembered that the sampling frequency of the original signal was 200 Hz. Then, a window of 500 samples would correspond to 2.5 seconds of information. Valuing the normal HR range in neonates, a normal value for the number of peaks would be 5 peaks.

Regarding the window length with which the calculation is made, it is proposed that the system updates data every 2.5 seconds, so, the data shown on the screen will contain the 2.5-second properly weighted information. As an example, if the HR value is 60 Hz, at least 200 samples are needed to detect a new heartbeat. According the HR range of neonates the mean value is 130 Hz, approximately. Therefore, a 2.5 seconds (500 samples) window length could detect enough number of peaks. Specifically, for a HR of 130 Hz we could get at least 5 peaks. With this consideration and solving in Equation 2.15 we would get an α value of 1/21.

As discussed in this section, extracting temporal information from cardiac events opens the door to the analysis of HR variability. Thus, with the signal shown in 2.19a, the interval function (2.19b) was calculated from the calculation of time differences between each beat detected with the *findpeaks* function. With this, we can evaluate how the HR is changing over time. Another statistical graph that can be used for the analysis of time difference signals between heartbeats is the histogram. A histogram whose morphology is similar to a normal distribution will correspond to a sinus rhythm, while a histogram with several concentrations of data will be expressing high variability and, therefore, possible pathologies associated with the heart. The record shown in figure 2.19 is very short and therefore the analysis of variability to be shown is not very inconclusive. Longer records would be needed for this purpose.

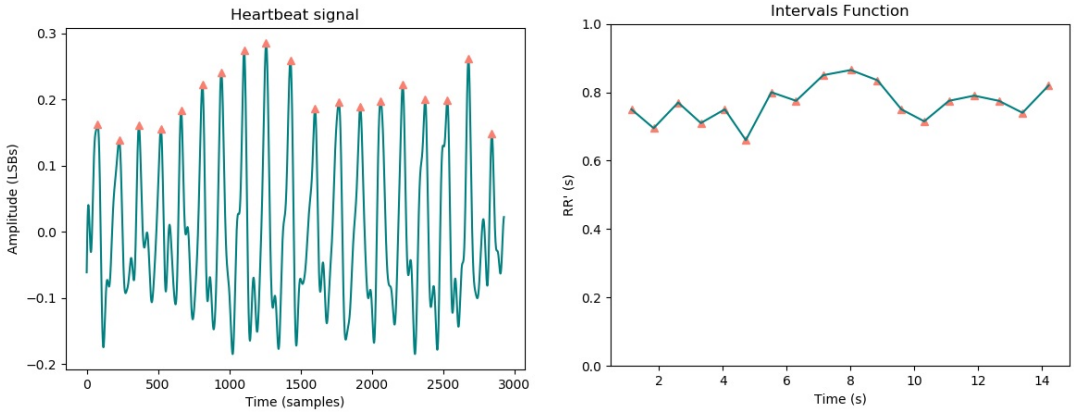

(a) **(b)**

Figure 2.19: a) Heartbeat signal. b) Intervals function of the heartbeat signal.

2.6 Stereo calibration

Calibration of the stereo pair was necessary to make the corresponding corrections in the stereo images for the obtention of the depth map reconstruction. For this purpose, a *Python* application was developed with the help of the *OpenCV* library and a checkboard pattern was used. This application allowed initializing the cameras, image acquisition and the calibration process. Once the calibration process was completed, a calibration file was generated; this file was later used for the reconstruction of the depth map representation. As described in the video acquisition protocol, the calibration file was generated just before the acquisition of the images of the neonates and in the same location and conditions. Figure 2.20 shows the checkboard pattern used during the calibration process. Figure 2.21 shows both the process of calibration and the calibration finished message displayed by the application.

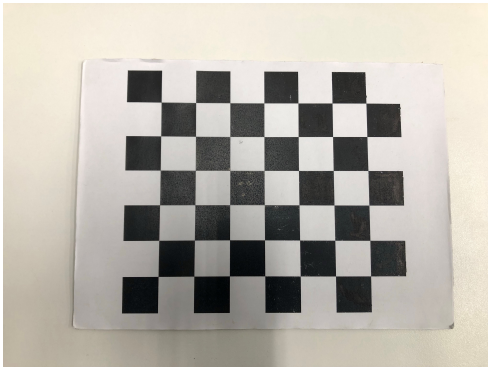

Figure 2.20: Checkboard pattern used for the stereo calibration process.

The application starts by turning on both cameras at the same time and searching a checkerboard pattern. The calibration process does not start until the checkerboard is found in the two images (left and right). Once the checkerboard is positioned so that both cameras can see it in the image, an image capture sequence begins at an acquisition frequency of 2 *Hz*. Then, the checkerboard should be moved and cover the full scene to guarantee good calibration. The acquisition process ends when 50 images have been captured by both cameras. The images are stored

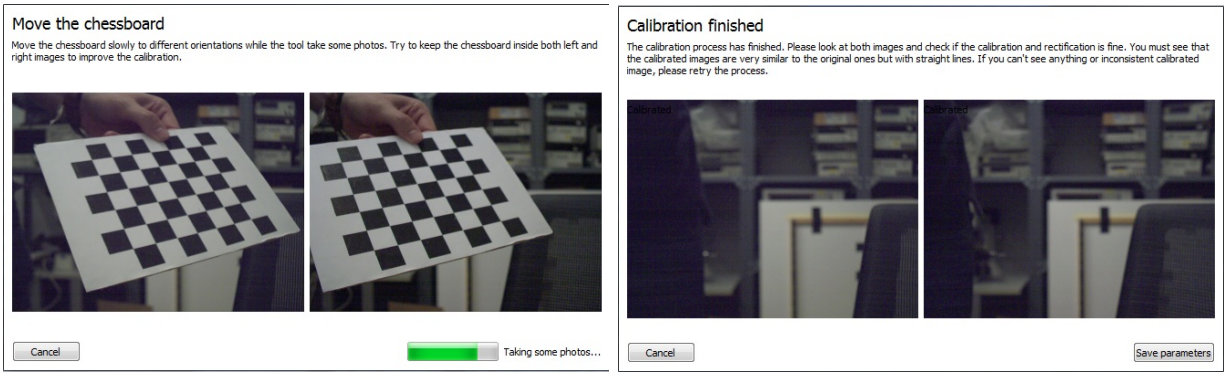

(a) Calibration process. **(b)** Calibration process finished.

Figure 2.21: Calibration process: a) Calibration in progress. b) Calibration finished.

and analyzed. First, the *findChessboardCorners* function is in charge of finding the corners of the checkerboard; this function stores both the analyzed image and the points where the corners are. These points are used later with the *stereoCalibrate* function in order to get the parameters needed to do the rectifications with *stereoRectify* function. In order to give a feedback of the process when it is finished the *"Calibration finished"* message appears and the two windows of the application show both the original images and the calibrated images.

2.7 Depth map techniques for BR estimation

One of the most outstanding features of the monitoring system presented in this work is the use of 2 cameras. Just as for the estimation of HR only one of the two cameras was necessary to extract the desired characteristics, in this section we use depth to estimate BR. In order to calculate the depth of a scene we use stereo imaging techniques that provide the necessary information to show a representation of the depth on a two-dimensional plane (for example: *depth map*). Thus, working with the 2 cameras gives you two images: the stereoscopic pair needed to generate a graphic representation of the depth of a scene. Table 2.3 shows the configuration of the cameras so that the acquisition of the images is simultaneous. The way in which the cameras are placed in the proposed modular structure is described in section 2.1. In figure 2.22, the results of a depth map generation algorithm are shown.

In the above-mentioned algorithm, they generated a representation of the depth from two images (stereo pair). To do this, they estimated the depth using pixel matching with *Sum of Absolute Differences*, setting a threshold of 2.5 % tolerance for which one pixel of the left image corresponded to the right image. In addition, they applied techniques to solve conflicts with pixels of the left image that had relation with those of the right image but that already matched with others.

In our project, the purpose of generating depth maps from the images of each camera was to extract breathing information. When we perform the action of breathing, we bring air into the lungs by increasing the volume of the rib cage; this causes movement and volume changes. Specifically, as the volume of the rib cage increases (inspiration), the distance between the torso and the cameras decreases, and as the volume of the rib cage decreases (expiration), this distance

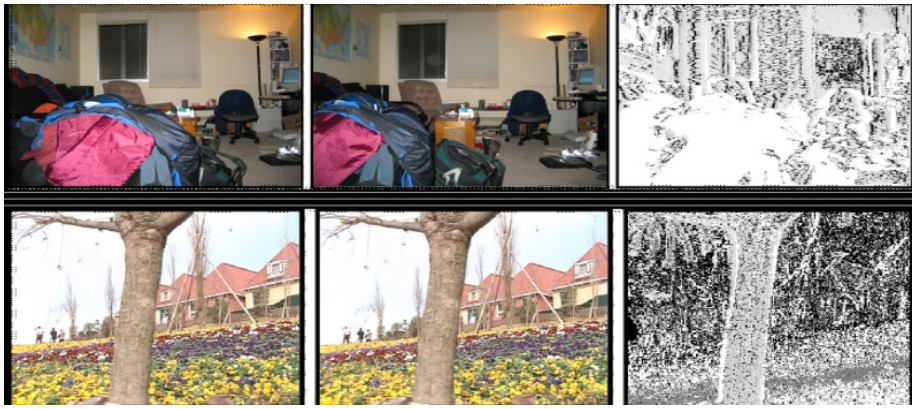

Figure 2.22: From left to right: Left image, right image and depth map generated (Aslam, Ansari, et al. 2019).

increases to a maximum value. By studying these effects over time, a signal can be obtained which is directly related to the subject's breathing.

For this purpose, an application was developed in *Python* and using the *OpenCV* library (see figure 2.23). The developed application is based on the modified *Hirschmuller's* algorithm used in the *OpenCV* functions (Hirschmuller 2007).

As far as the user interface is concerned, the application has a toolbar at the top with the following options: load calibration parameters, load the video generated with both the left and right camera, play the videos and save the depth map as a video sequence. The box on the left is where all the parameters needed to modify the generation of the depth map are. These parameters are predefined in the *OpenCV* library. These parameters are followed by two more parameters that allow you to set the black and white levels. If the white level is *255* and the black level is *0*, it means that the closest object will be represented in white and the furthest object in black. In the box on the right, the space is divided into 3 smaller boxes. In the box at the top left is where, when loading the video from the left camera, the first frame is displayed. The top right box is where, when loading the video from the right camera, the first frame is displayed. The largest frame is where the resulting representation of the depth is shown frame by frame.

For the generation of the representation of the depth it is necessary to modify the parameters that are located in the left box. The modification of these parameters was done on the basis of the documentation offered by *OpenCV* website in which some values and ranges of values are specified. As mentioned at the beginning, the application contains the option of playing the videos; once the image reconstructed from the stereo pair was appropriate, the video was played and the sequence of depth map images corresponding to each frame was saved in another video *.avi* file.

In terms of how the depth map in the larger box of the interface was generated, *OpenCV* was used too. First, the calibration file containing the necessary parameters was used to rectify the images if necessary. The rectification was performed for both images with the function *initUndistortRectifyMap*. Once this was done, the function *StereoSGBMcreate* creates the depth map from the values of the modified parameters that appear on the left side of the application interface.

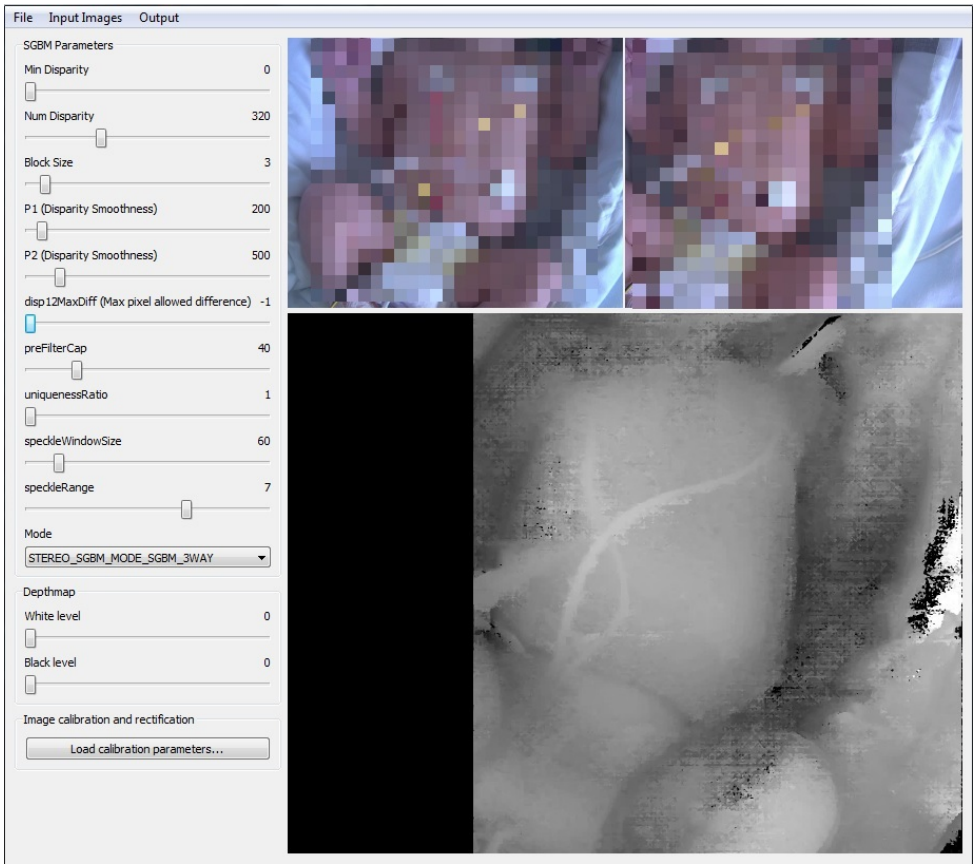

Figure 2.23: Stereo depth map application. (Image blurred due to GDPR requirements).

2.7.1 ROI Location

In order to find information related to breathing it is necessary to analyze the depth map which is a pseudo-color gray image where depth is encoded as a gray value. Since this representation is constructed on a one-color map and the depth of objects will be defined by the value of that color, it would suffice to study how it changes over time. It is necessary to make a study to define which region of the body is more suitable to obtain the breathing signal. In neonates, the breathing movement is more pronounced in the abdominal region than in the pectoral region. In addition, unlike adults, breathing in neonates is irregular (Mejía and Daza 2011). Therefore, signs can be expected in which these irregularities will be reflected.

For the study of the location of the *ROI*, two regions have been proposed which are, in principle, the areas that will see most reflected that breathing signal: the chest and abdomen. Regarding the size of the *ROI* to evaluate the signal, the restriction is lower, since the acquisition frequency was lower and, therefore, the volume of data to be processed is also lower. The process by which depth changes are analyzed is based on the average color change of the pixels included in the selected *ROI*. This is done in a similar way to the technique described in subsection 2.5.1, but this time only one color is analyzed. The video to be processed is a three-dimensional matrix, in which the first two dimensions represent the width and height as defined in Equation 2.18 , and the third dimension is the number of frames that formes the video. The *width* and *height* is

limited by the *ROI*. Regarding the change in color (depth) for the image over time, each average of the *ROI* of side *n*x*k* for *l* frames has been calculated (Equation 2.19).

$$W = \begin{pmatrix} w_{11} & w_{12} & w_{13} & ... & w_{1j} \\ w_{21} & w_{22} & w_{23} & ... & w_{2j} \\ ... & ... & ... & ... & ... \\ w_{i1} & w_{i2} & w_{i3} & ... & w_{ij} \end{pmatrix} \tag{2.18}$$

$$x_W(l) = \frac{1}{n}\frac{1}{k}\sum_{i=1}^{n}\sum_{j=1}^{k} x_{Wij}(l) \tag{2.19}$$

Table 2.8 shows the characteristics of the selected locations to be processed and figure 2.25 shows where are the *ROI*s placed.

Body Area	**ROI Width** (pixels)	**ROI Height** (pixels)	**Frame Rate** (fps)
Chest Abdomen	200	200	30

Table 2.8: Video data for finding the best ROI location.

(a) **(b)**

Figure 2.24: ROI location assessment: a) Chest. b) Abdomen.

For the evaluation of signal quality, the same parameters were taken into account as in the section in which the *ROI* location study was performed to find the best *HR* signal. This time, the BR signals generated in the chosen locations were studied. The parameters were: amplitude of the signal in *LSBs*, value of the highest peak in the frequency spectrum in *dB* and in *Hz*, value of the second highest peak in *dB* and in *Hz*, value of the difference between the highest peak and the second highest peak in *dB*, and the *signal-to-noise ratio*. The difference between the highest peak in *dB* and the second highest peak in *dB* is defined in Equation 2.8 and the *signal-to-noise ratio* is defined as the difference between the highest peak in *dB* and the *Noise Floor* value in *dB* (Equation 2.9). The results of *ROI location* analysis are shown in subsection 3.3.1.

2.7.2 ROI Size

As in the previous section, the choice of the size of the *ROI* is based on the study of the quality of the signal generated in that region. However, the acquisition frequency defined for the extraction of the breathing signal was much lower than the acquisition frequency for the extraction of HR information. This implies a much smaller number of data stored per second. All this meant that the choice of *ROI* size was not as critical and demanding as in the other application. However, a study of the quality of the signal was made. Therefore, once the region where the best results were obtained was chosen, different *ROI* size values were analyzed. The parameters that were taken into account to determine the quality of the signal were: amplitude of the signal in *LSBs*, value of the highest peak in the frequency spectrum in *dB* and in *Hz*, value of the second highest peak in *dB* and in *Hz*, value of the difference between these two peaks in *dB*, the *signal-to-noise ratio* and the mean value of the *standard deviation matrix* of the *ROI*.

Video n°	**Body Area**	**ROI Width** (pixels)	**ROI Height** (pixels)	**Frame Rate** (fps)
1	Abdomen	400	400	30
2		300	300	
3		200	200	
4		100	100	
5		50	50	
6		20	20	

Table 2.9: Video data for finding the best ROI location.

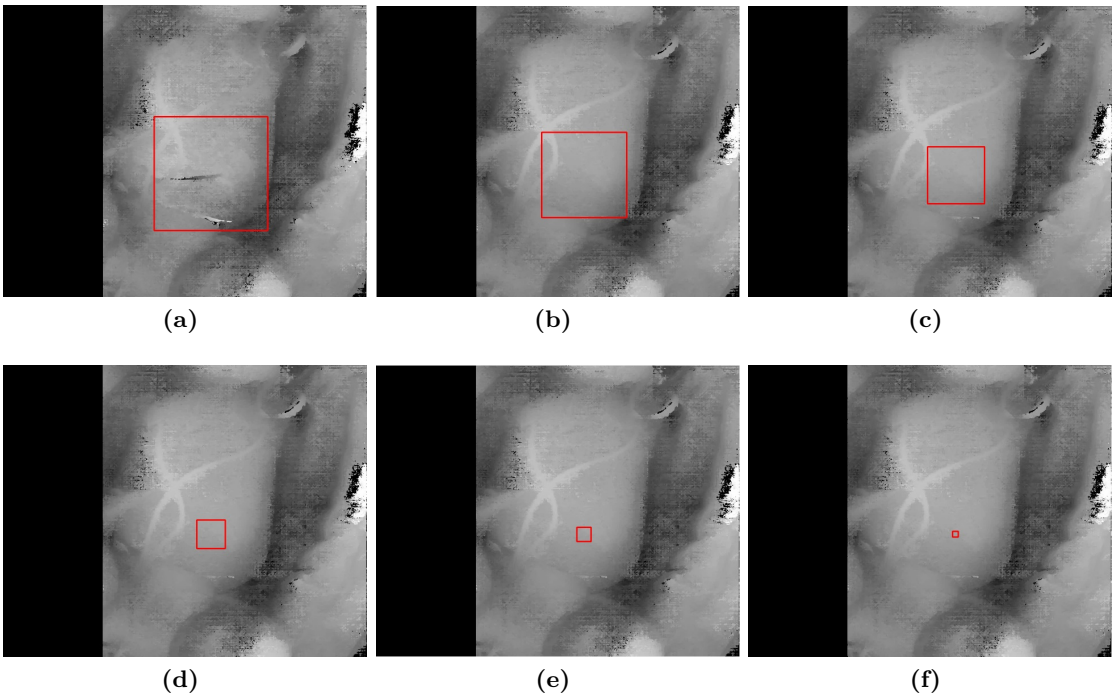

Figure 2.25: ROI size assessment: a) 400x400. b) 300x300. c) 200x200. d) 100x100. e) 50x50. f) 20x20.

2.7.3 Signal Processing

The processing procedure followed for the extraction of respiratory information was practically the same as that followed for the extraction of the cardiac signal, except that it was split in two stages. This procedure is described in subsection 2.5.3. The differences are the value of cut-off frequencies of both low-pass and high-pass filters. The first stage was identical. The bandwidth that was determined to obtain the desired heartbeat signal information was based on the HR range found in the literature. The same was done for respiratory information. In the literature, and as commented in the introduction, the normal respiratory rate range in neonates is between 33 and 55 breaths per minute; that is, between 0.5 and 0.9 *Hz* approximately. Therefore, the bandwidth to obtain the information of interest was set between 0.25 and 2 *Hz* so that, in case the respiratory frequency exceeded the normal values both above and below, the correct information could also be obtained. The filter response is defined in Equation 2.12 and the block diagram of the signal processing procedure can be seen in figure 2.17. Moreover, the output signals of the 3 signal processing stages are plotted in figure 2.26.

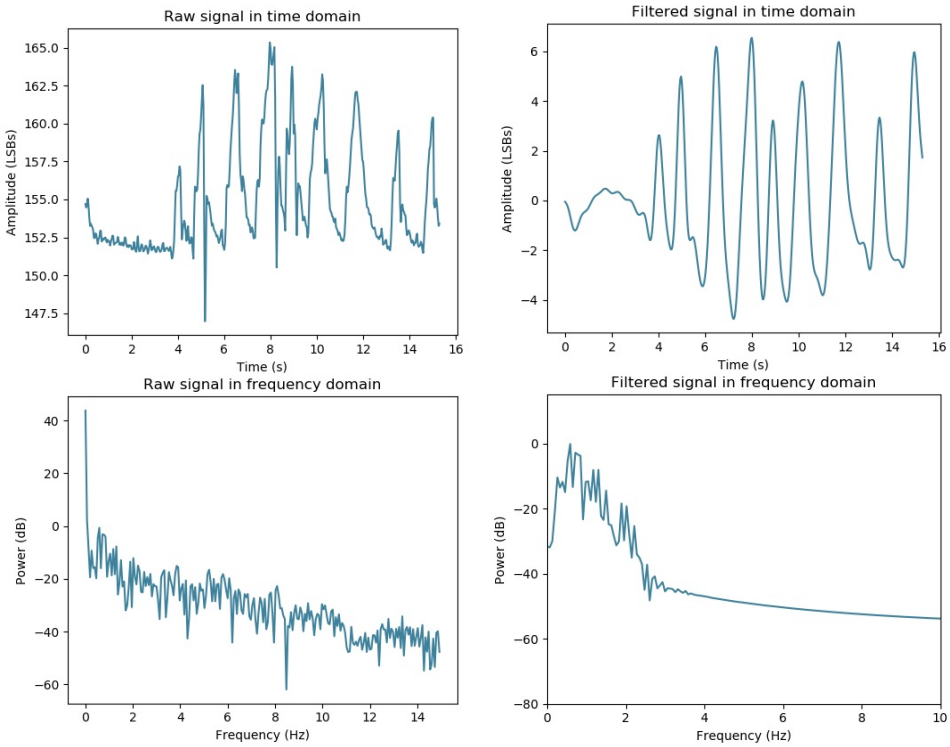

Figure 2.26: Breathing signal obtained in the abdomen area. In the top graphs the signal is shown in the time domain and in the bottom graphs in the frequency domain. **a)** Original signal. **b)** Filtered signal.

2.7.4 BR estimation

With regard to the estimation of the respiratory rate, the same methods were followed as for the estimation of the HR. These methods are described in subsection 2.5.4. In addition, it has also been proposed to make a study of the time series that establishes the time differences between consecutive breaths. This, also opens the door to the study of respiratory rate variability. The purpose of this type of study is to find possible pathologies related to the changes in the BR. In newborns, breathing is usually irregular and even more so at such early ages. Analyzing these temporal differences, both agitated and slow breathing can be detected. You can even see when the baby has stopped breathing. If we look at the records obtained with the stereo pair system we can see that at the beginning of the signal there is no change in depth, but only small movements typical in newborns. It can be determined that, in that period of up to 4 seconds, the newborn stopped breathing.

As for displaying a value on screen with the respiratory frequency information we followed the two strategies proposed, but with different values of the window and its displacement. The acquisition frequency of the original signal was 30 Hz. If the respiratory frequency was 60 breaths per minute, at least 30 samples would be needed to see a maximum in the signal that determined the action of breathing. Unlike the heart, respiration is a movement that is controlled both voluntarily and involuntarily; this can determine that the variability that the system would have if the calculation of the value to be shown were the last breathing interval could be much higher. In addition, the fact that the acquisition frequency is 30 Hz implies a lower volume of data. Therefore, a time window is proposed for calculating the moving average of 10 seconds, i.e. 300 samples and a displacement of the moving average of 5 seconds, i.e. 150 samples. The equations used to calculate both the time differences between consecutive breaths and the proposed value to be displayed on the screen according to the two strategies can be seen in Equation 2.13, Equation 2.14, Equation 2.15 and Equation 2.17. This time in Equation 2.13, p_{t+1} is the value of the subsequent breathing peak position and p_t is the value of the current breathing peak position. So, in this way we obtain the mentioned intervals function of the respiratory events. In Equation 2.14, α it the constant weight we apply, x_{n-1} is the previous HR value, P is the number of found peaks and b_i is the value of each founded peak interval.

Chapter 3

Results

3.1 Camera calibration

3.1.1 Homogeneity study

Assessment of the region of interest (ROI)

In general, as the lower rows of figures *3.1, 3.3, 3.5, 3.7* and *3.9* show, the homogeneity study reveals no clear noise pattern but a pattern in which the right side of the *ROI* has higher values than the left side. That behavior is repeated for each set of integration time and light source current values and for each *RGB* channel. This may be due to a non-homogeneity integrating sphere (accepted hypothesis by the image laboratory technician) or due to misplacement of either the camera or light source. Regarding the noise of each *RGB* channel and at first sight, the color map (upper row of the figures *3.1, 3.3, 3.5, 3.7* and *3.9*) suggests that the blue channel is noisier than the red and green channels, with the green channel being the least noisy channel. Actually, the suggestions are evidenced in tables *3.1, 3.2, 3.3, 3.4* and *3.5*. The upper row of *figure 3.1* shows the standard deviation matrix for each channel (each column). The vertical and horizontal axis are the height and the width values of the *ROI* and the range of the color map values is common for all the channels, where the lowest value is the minimum value of the three matrices and the highest value is the maximum value of the three matrices. In this way, establishing common boundaries makes it easier to visually appreciate differences. The lower row of *figure 3.1* shows the average matrices for each channel (each column). Same way, vertical and horizontal axis are the height and the width values of the *ROI* but the range of the color map values is different for each channel, where the lowest value of each matrix is its minimum value and the highest value of each matrix is its maximum value. The figures *3.2, 3.4, 3.6, 3.8* and *3.10* show the distribution of the pixel values (upper row) and the standard deviation frame by frame (lower row). The vertical and horizontal axis of the graphics in the lower rows are standard deviation values and frame number, respectively.

In tables *3.1, 3.2, 3.3, 3.4* and *3.5* all the described parameters are shown. First column *(Channel)* corresponds to the RGB channel name; the next one *(STD)* corresponds to the standard deviation of the mean pixel matrix; the next one *(Mean STD)* is the mean standard deviation value of the standard deviation matrix; the next two columns (*Min STD* and *Max STD*) are the minimum and maximum standard deviation values of the standard deviation matrix; the last column *(Color AVG)* refers to the color average value.

Integrating Time: 5 ms, Light current: 0.005 mA					
Channel	STD	Mean STD	Min STD	Max STD	Color AVG
RED	1.83	1.75	1.62	1.91	231.48
BLUE	2.06	3.63	3.3	4.16	144.01
GREEN	1.49	1.44	1.3	1.64	197.46

Table 3.1: Homogeinity study results for a 5 ms integration time and a 0.005 mA light current.

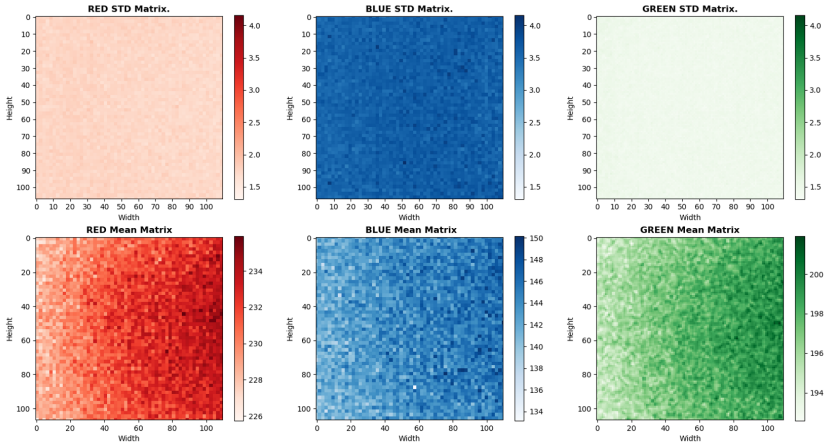

Figure 3.1: Standard deviation matrix for each RGB channel (upper row). Mean pixel values over the time matrix for each RGB channel (lower row). Integration time: 5 ms. Light current: 0.005 mA.

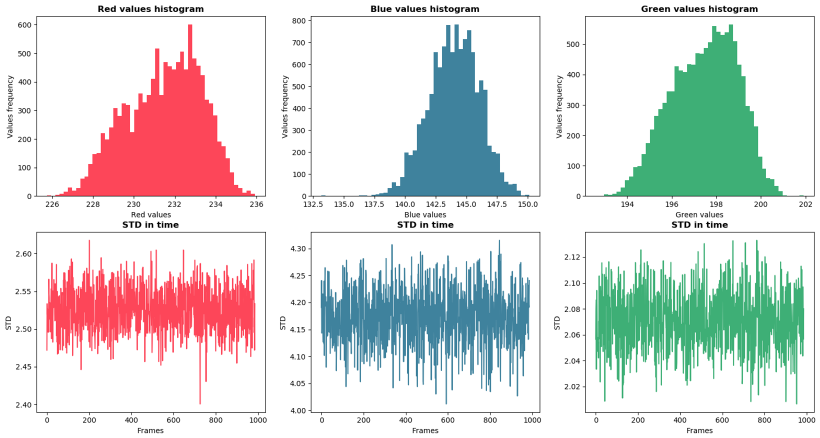

Figure 3.2: Distribution of the mean color values for each RGB channel (upper row). Standard deviation frame by frame for each RGB channel (lower row). Integration time: 5 ms. Light current: 0.005 mA.

integration Time: 3.125 ms, Light current: 0.008 mA					
Channel	STD	Mean STD	Min STD	Max STD	AVG color value
RED	1.95	1.72	1.57	1.95	243.07
BLUE	1.96	3.43	3.15	4.08	152.54
GREEN	1.68	1.44	1.31	1.57	207.78

Table 3.2: Homogeinity study table results for a 3.125 ms integration time and a 0.008 mA light current.

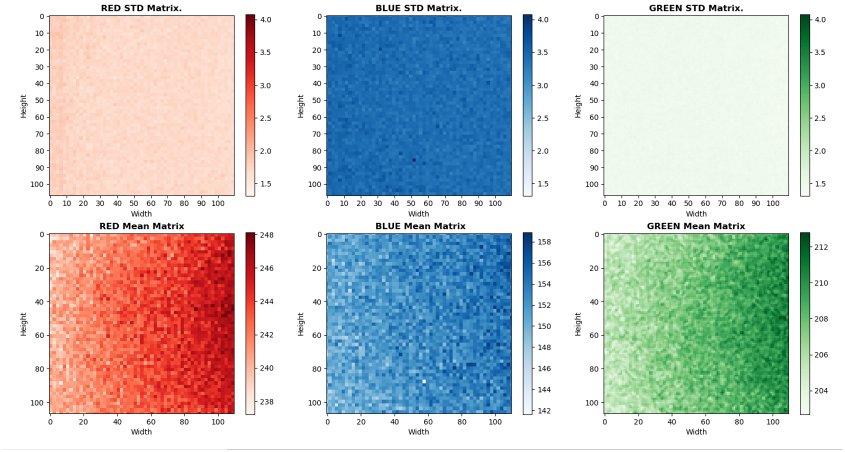

Figure 3.3: Standard deviation matrix for each RGB channel (upper row). Mean pixel values over the time matrix for each RGB channel (lower row). Integration time: 3.125 ms. Light current: 0.008 mA.

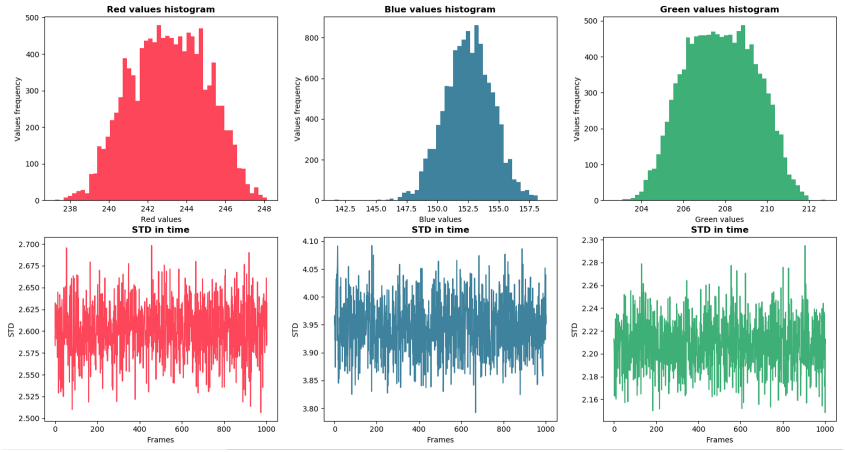

Figure 3.4: Distribution of the mean color values for each RGB channel (upper row). Standard deviation frame by frame for each RGB channel (lower row). Integration time: 3.125 ms. Light current: 0.008 mA.

Integration Time: 2.5 ms, Light current: 0.01 mA					
Channel	STD	Mean STD	Min STD	Max STD	AVG color value
RED	1.98	1.77	1.59	1.96	239.88
BLUE	1.98	3.45	3.13	3.93	150.68
GREEN	1.63	1.44	1.31	1.61	205.16

Table 3.3: Homogeinity study results for a 2.5 ms integration time and a 0.01 mA light current.

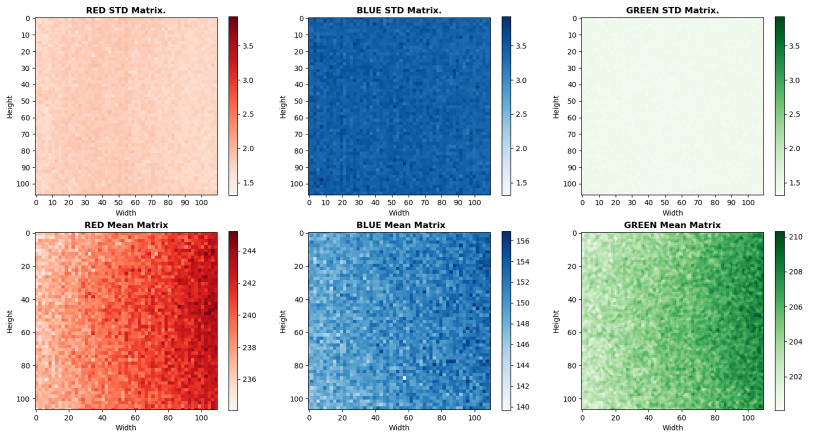

Figure 3.5: Standard deviation matrix for each RGB channel (upper row). Mean pixel values over the time matrix for each RGB channel (lower row). Integration time: 2.5 ms. Light current: 0.01 mA.

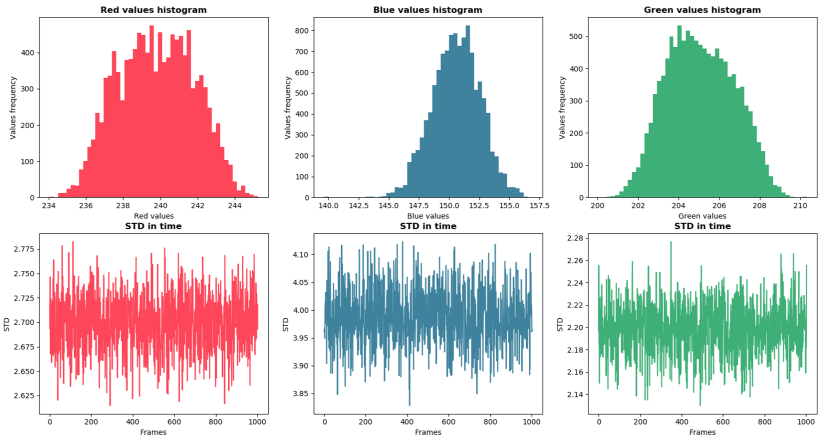

Figure 3.6: Distribution of the mean color values for each RGB channel (upper row). Standard deviation frame by frame for each RGB channel (lower row). Integrating time: 2.5 ms. Light current: 0.01 mA.

Integrating Time: 1.563 ms, Light current: 0.016 mA					
Channel	STD	Mean STD	Min STD	Max STD	AVG color value
RED	2.12	1.7	1.54	1.85	245.44
BLUE	2.11	3.45	3.17	3.95	154.63
GREEN	1.83	1.3	1.3	1.58	210.28

Table 3.4: Homogeinity study results for a 1.563 ms integration time and a 0.016 mA light current.

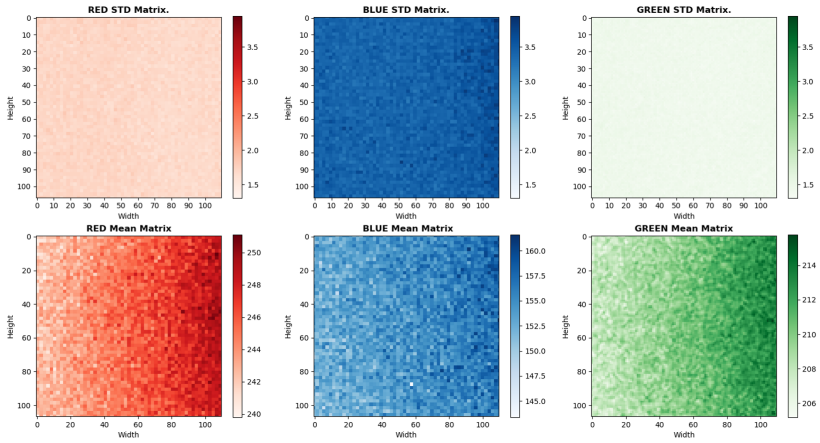

Figure 3.7: Standard deviation matrix for each RGB channel (upper row). Mean pixel values over the time matrix for each RGB channel (lower row). Integration time: 1.563 ms. Light current: 0.016 mA.

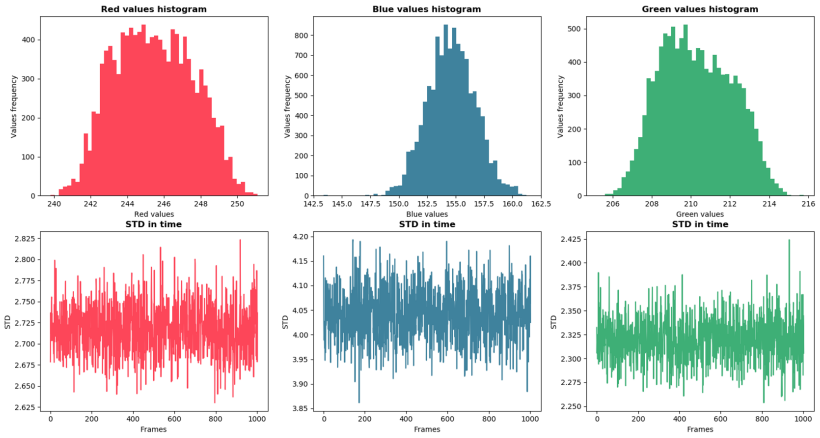

Figure 3.8: Distribution of the mean color values for each RGB channel (upper row). Standard deviation frame by frame for each RGB channel (lower row). Integration time: 1.563 ms. Light current: 0.016 mA.

Integration Time: 1.25 ms, Light current: 0.02 mA					
Channel	STD	Mean STD	Min STD	Max STD	AVG color value
RED	2.18	1.71	1.56	1.92	244.04
BLUE	2.09	3.43	3.16	3.86	153.87
GREEN	1.88	1.43	1.3	1.57	209.14

Table 3.5: Homogeinity study results for a 1.25 ms integration time and a 0.02 mA light current.

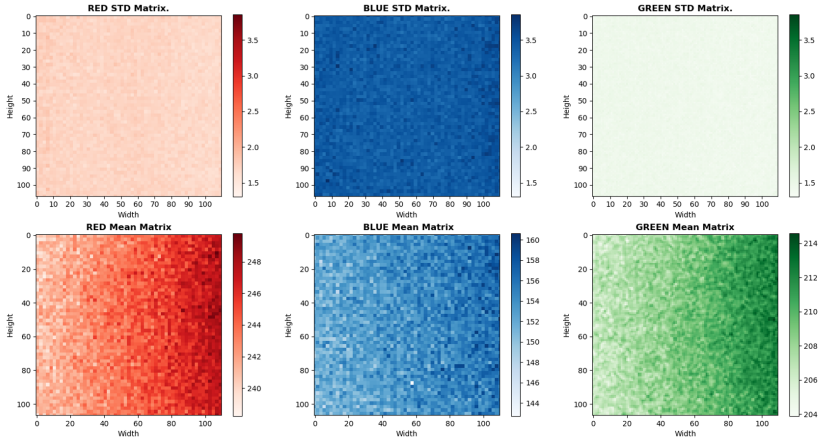

Figure 3.9: Standard deviation matrix for each RGB channel (upper row). Mean pixel values over the time matrix for each RGB channel (lower row). Integration time: 1.25 ms. Light current: 0.02 mA.

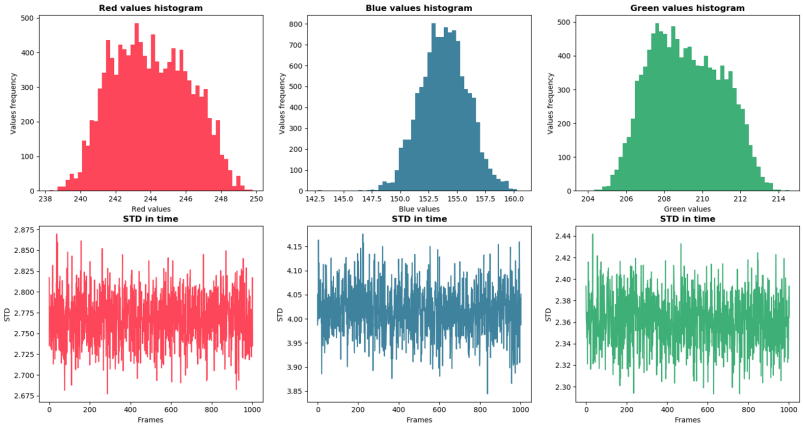

Figure 3.10: Distribution of the mean color values for each RGB channel (upper row). Standard deviation frame by frame for each RGB channel (lower row). Integration time: 1.25 ms. Light current: 0.02 mA.

Assessment of a single point at the center of the ROI

The assessment of a single pixel in the green channel and at the center of the *ROI* over time and is shown in figures *3.11, 3.12, 3.13, 3.14* and *3.15*. The pixel has not steady values since they are oscillating between the values included in the *table 3.6*.

IT (ms)	LC (mA)	Mean	Min	Max	STD
5	0.005	198.26	194	203	1.436
3.125	0.008	208.35	204	213	1.53
2.5	0.01	205.53	201	211	1.451
1.563	0.016	210.66	206	216	1.412
1.25	0.02	209.37	205	214	1.44

Table 3.6: Homogeneity study results for a single point for different integration time and light source current values.

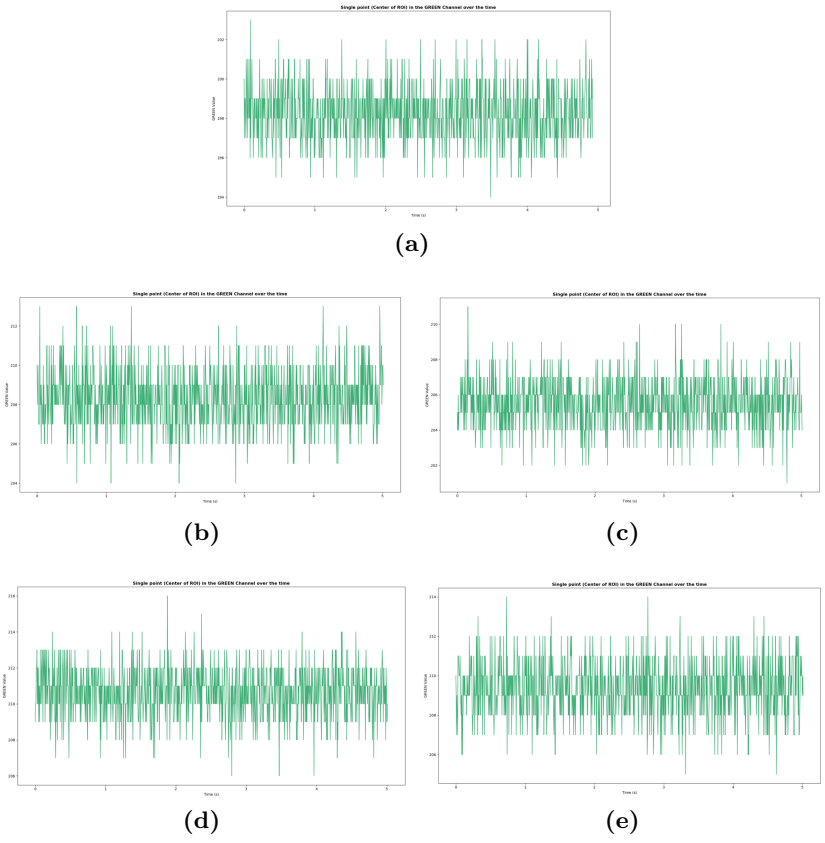

Figure 3.11: Homogeneity study results for a single point in the green channel for different integrating time *(IT)* and light source current *(LC)* values. **a)** IT = 5 ms. LC = 0.005 mA; **b)** IT = 3.125 ms. LC = 0.008 mA; **c)** IT = 2.5 ms. LC = 0.01 mA; **d)** IT = 1.563 ms. LC = 0.016 mA; **e)** IT = 1.25 ms. LC = 0.02 mA

3.1.2 Linearity study

Temperature curve and gray level

Regarding the temperature curve showed in figure 3.13, the temperature initially increases rapidly from ambient temperature values *(25 °C)* to *45 °C* in less than 3 minutes. Then, the values start to stabilize at *50 °C*. In order to check the dependence between the temperature and the output level and possible noise, an assessment of the gray level in a region is included in figure 3.12. The outcomes do not reveal a special influence in the camera output during the warm-up period of time, as the oscillation of the values remains throughout the test. It should be noted two distortion or deformation signal events in the intervals from 450 to 550 seconds and from 600 to 800 seconds occur due to unknown reasons.

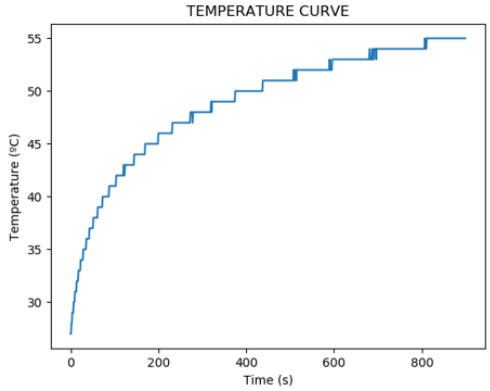

Figure 3.12: Temperature curve of the camera for fifteen minutes.

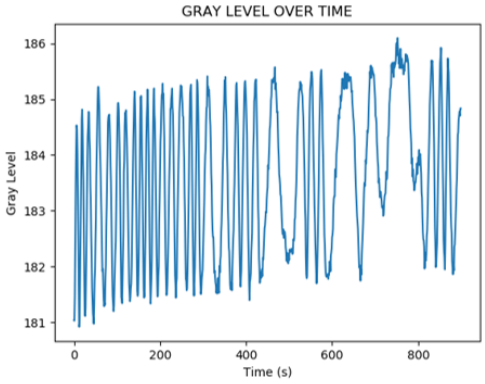

Figure 3.13: Gray mean values of a region for fifteen minutes.

The results of the second part of the linearity study, the analysis of the integrating time and light source current effect, are shown in *figure 3.18*. It is assumed that the light source current gives a steady and constant response and the integrating time establishes a time window with the values of *table 3.7*. Thus, if there is a linear behaviour of the system, the output signal (color intensity or mean color value) would remain constant in time; as shown in *figure 3.18*, this hypothesis is not met and the system has a certain non-linearity response. The values in red are the minimum and the maximum color average value for the three RGB channels. IT is *integration time*, LC is *Light source current*, and Color AVG is the *mean color value*.

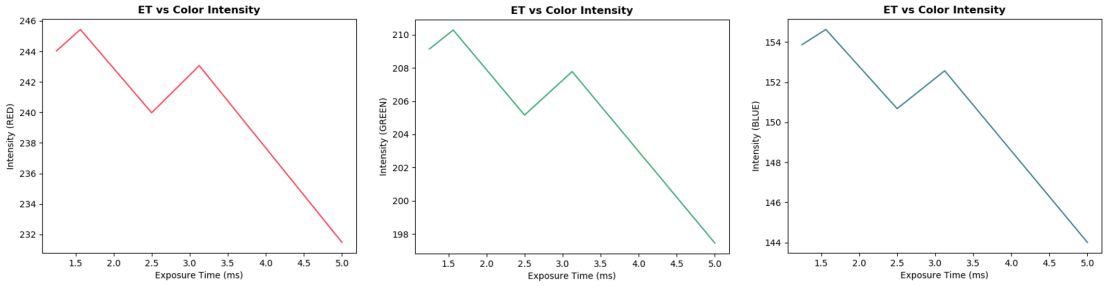

(a) **(b)** **(c)**

Figure 3.14: Linearity study for the each of the three RGB channels and for five different integration time values. **a)** Red channel; **b)** Green channel; **c)** Blue channel.

RED			GREEN			BLUE		
IT (ms)	LC (mA)	Color AVG	IT (ms)	LC (mA)	Color AVG	IT (ms)	LC (mA)	Color AVG
5	0.005	231.48	5	0.005	197.46	5	0.005	144.01
3.125	0.008	237.07	3.125	0.008	207.75	3.125	0.008	152.54
2.5	0.01	239.98	2.5	0.01	205.16	2.5	0.01	150.68
1.563	0.016	245.44	1.563	0.016	210.28	1.563	0.016	154.63
1.25	0.02	244.04	1.25	0.02	209.14	1.25	0.02	153.87

Table 3.7: Linearity results for the three RGB channels and for five different integration time values.

3.2 Color techniques

This section presents the results related to the location of the ROI, the justification of the size of the ROI, and the results related to the detection of HR by color change analysis.

3.2.1 ROI Location

Table 3.8 and table 3.9 show the results of the *ROI* location analysis. As we show, the left chest area is the area yielding the highest quality results. In reference to the amplitude analysis in the different chosen areas, in the left chest area there is a great difference with respect to the rest of the regions; in that area the value is almost double the second maximum value achieved. On the other hand, regarding to the analysis of the frequency spectrum, in the signal acquired in the abdomen area a value of SNR has been obtained virtually equal to that obtained in the left chest area. The problem with the abdomen area is that the second highest peak was very close to the first and that is why the value of the difference between the two highest peaks is so low. In the left chest area both the *SNR* value and the difference between highest two peaks are reasonably better than in other regions. Therefore, it is established that the region in which the signal is seen with the highest quality is the left chest area. The values confirming this are framed in green in table 3.8 and table 3.9. The values shown in the first table are (from left to right): the location of the *ROI*, the peak-to-peak amplitude of the signal (*APP*), the highest peak of the frequency spectrum in decibels and hertz (HP_1), the second most energetic peak in the frequency spectrum in decibels and hertz (HP_2), and the noise floor energy value in decibels (*NFP*). The values shown in the second table are (from left to right): the location of the *ROI*, the energy difference in decibels between the most energetic frequency peak and the second most energetic peak (ΔHP) and the signal-to-noise ratio (*SNR*).

Following the tables, the graph corresponding to the processed system output signal are shown (figure 3.15, figure 3.16, figure 3.17 and figure 3.18). Specifically, the signal of the green channel is shown in the time domain and its corresponding frequency spectrum. The frequency range of the spectrum graph is delimited between 0 and 10 *Hz* to make it easier to display the results in the frequency domain.

ROI Location	**APP** (LSBs)	$\mathbf{HP}_1$ (dB)	$\mathbf{HP}_1$ (Hz)	$\mathbf{HP}_2$ (dB)	$\mathbf{HP}_2$ (Hz)	**NFP** (dB)
Left Chest	0.43	-22.23	1.88	31.21	2.31	-55.01
Right Chest	0.18	-29.41	1.75	-35.02	2.19	-51.65
Sternum	0.25	-28.18	1.88	-33.12	1.34	-51.82
Abdomen	0.24	-23.69	2.02	-24.48	1.78	-55.08

Table 3.8: Results of the ROI location assessment.

ROI Location	**ΔHP** (dB)	**SNR** (dB)
Left Chest	8.97	32.73
Right Chest	5.61	23.62
Sternum	4.94	23.64
Abdomen	1.48	31.39

Table 3.9: Results of the ROI location assessment.

- ***Left chest***.

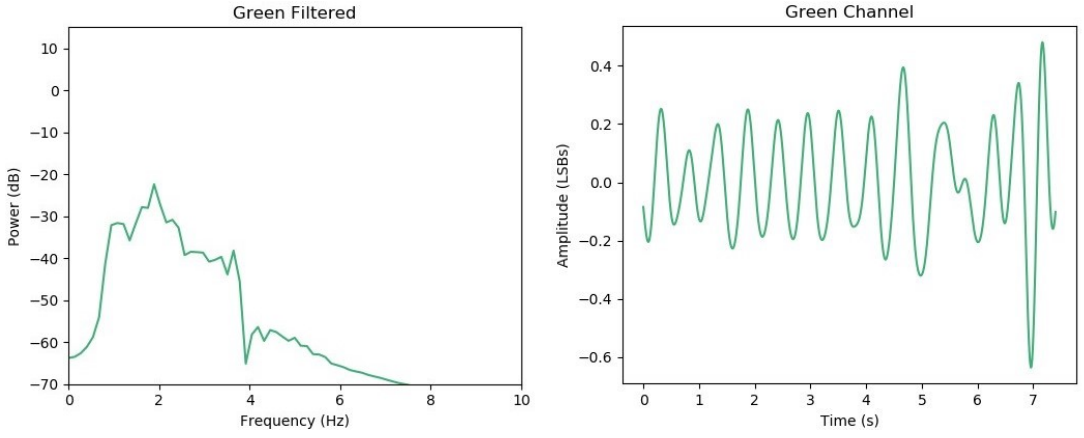

(a) **(b)**

Figure 3.15: Signal of the green channel calculated for the left chest ROI. **a)** Frequency spectrum of the signal; **b)** Signal in the time domain.

- ***Right chest***.

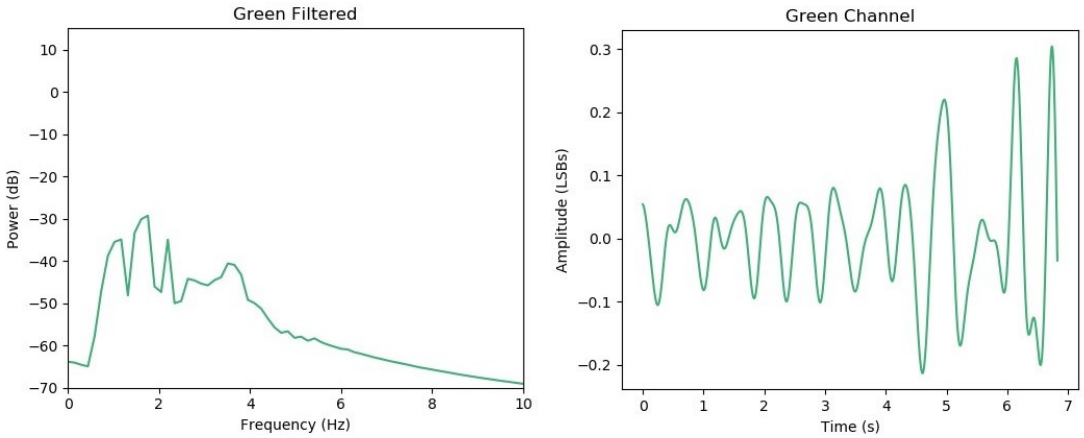

(a) **(b)**

Figure 3.16: Signal of the green channel calculated for the right chest ROI. **a)** Frequency spectrum of the signal; **b)** Signal in the time domain.

- ***Sternum***.

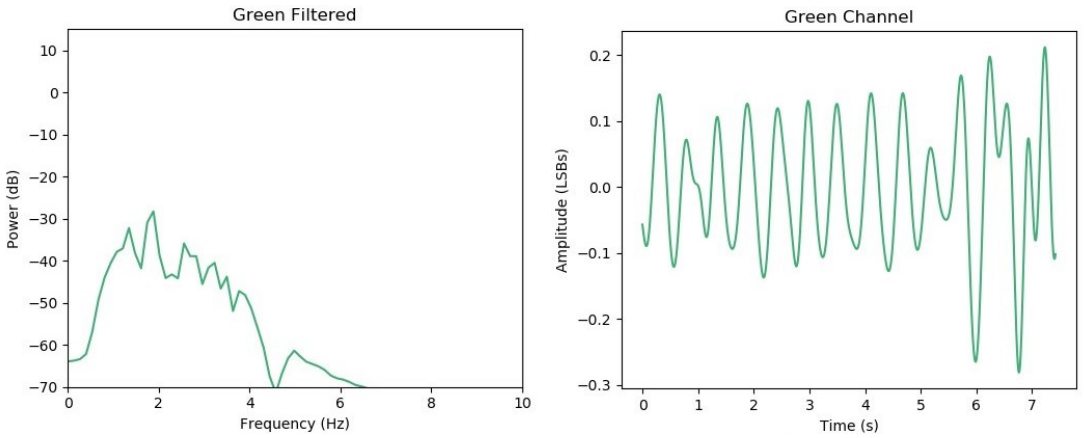

(a) **(b)**

Figure 3.17: Signal of the green channel calculated for the sternum ROI. **a)** Frequency spectrum of the signal; **b)** Signal in the time domain.

- ***Abdomen***.

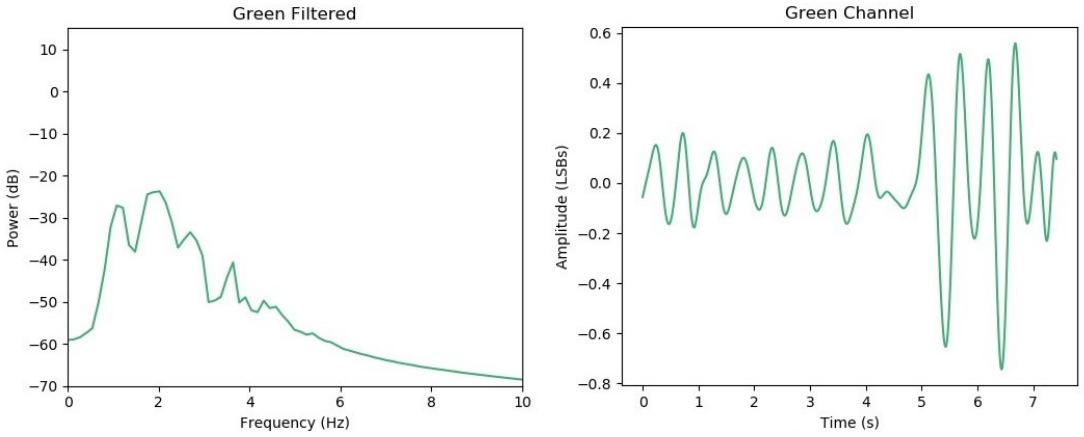

Figure 3.18: Signal of the green channel calculated for the abdomen ROI. **a)** Frequency spectrum of the signal; **b)** Signal in the time domain.

3.2.2 ROI Size

The results of the study of the optimal size of the ROI are shown in table 3.10 and table 3.11. As can be seen, the smaller the *ROI* the lower the value of the standard deviation (*SD*). The signal-to-noise ratio, the amplitude of the signal and the difference between the two strongest frequency peaks changes differently. A higher value of standard deviation could suggest that can be better appreciated, but if we check the 110x110 and 140x140 *ROI*s in the real image we find some objects that go inside de *ROI* sometimes and they increase de *SD* value. Moreover the APP in these *ROIs* are significantly lower than in the *80x80 ROI*, the higher ΔHP value is in the *80x80 ROI* and the *SNR* values are very close to the *80x80 ROI's* value. So, it looks like the best *ROI* size value is *80x80* since it has the highest *APP* and ΔHP values. Moreover in this *ROI* the *SNR* value is reasonable high as well as the *SD* value is substantially good too.

ROI Size (pixels)	**APP** (LSBs)	**HP**$_1$ (dB)	**HP**$_1$ (Hz)	**HP**$_2$ (dB)	**HP**$_2$ (Hz)	**NFP** (dB)
140x140	0.25	-28.18	1.88	-35.24	1.34	-56.99
110x110	0.41	-23.24	1.88	-30.31	2.31	-56.34
80x80	0.43	-22.23	1.88	-31.21	2.31	-55.01
60x60	0.41	-23.35	1.88	-30.87	1.21	-52.94
40x40	0.38	-23.91	1.88	-29.75	1.34	-50.43
20x20	0.32	-24.21	1.88	-28.63	1.34	-45.06

Table 3.10: Results of the ROI size assessment.

ROI Size (pixels)	**ΔHP** (dB)	**SNR** (dB)	**SD** (LSBs)
140x140	7.06	28.81	5.33
110x110	7.07	33.11	4.45
80x80	8.97	32.73	3.49
60x60	7.52	29.59	3.21
40x40	5.84	26.52	3.18
20x20	4.42	20.85	3.05

Table 3.11: Results of the ROI size assessment.

- ***Size 1: 140x140***.

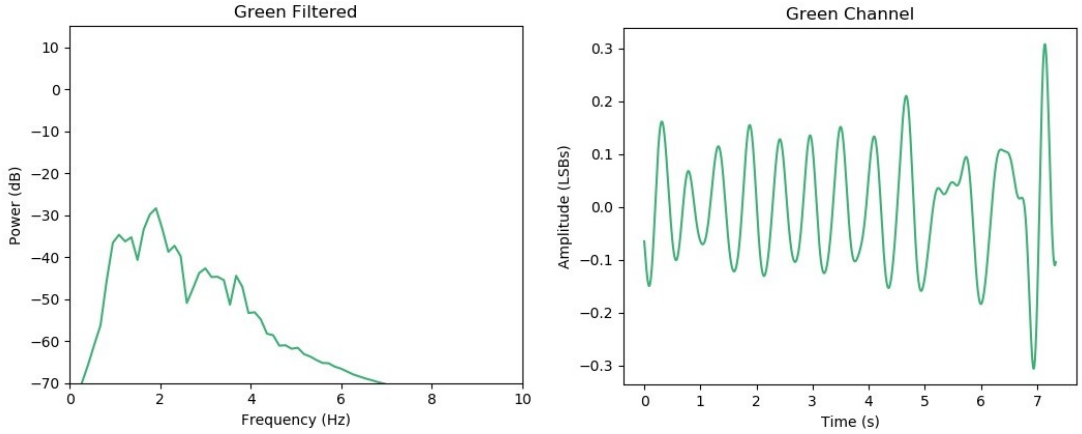

(a) **(b)**

Figure 3.19: Signal of the green channel calculated for the 140x140 ROI size. **a)** Frequency spectrum of the signal; **b)** Signal in the time domain.

- ***Size 2: 110x110***.

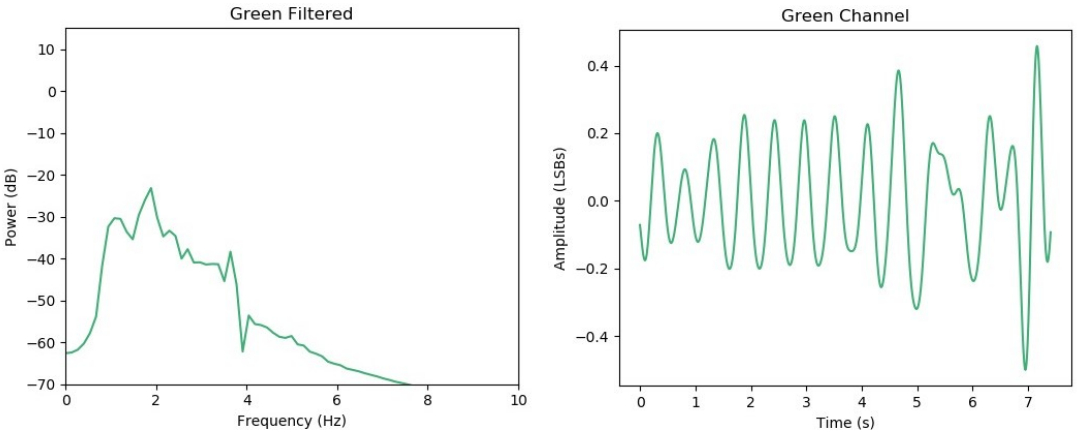

(a) **(b)**

Figure 3.20: Signal of the green channel calculated for the 110x110 ROI size. **a)** Frequency spectrum of the signal; **b)** Signal in the time domain.

- ***Size 3: 80x80***.

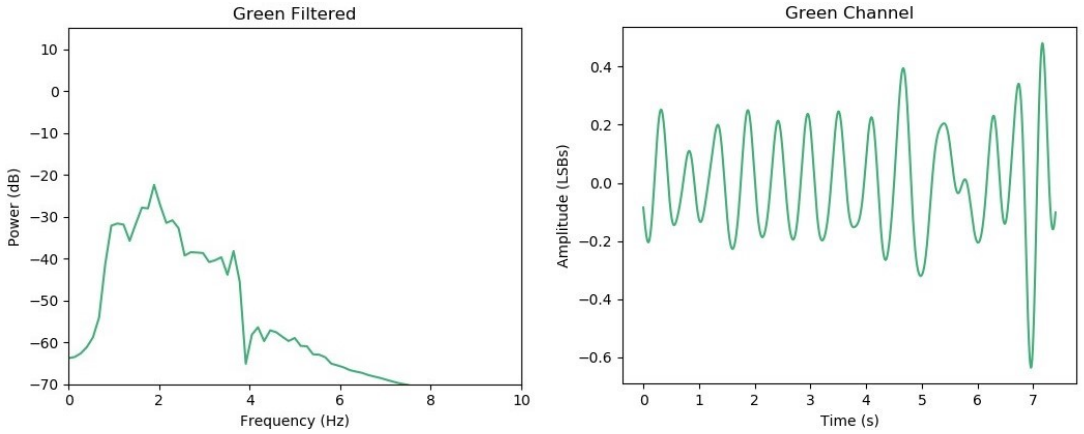

(a) **(b)**

Figure 3.21: Signal of the green channel calculated for the 80x80 ROI size. **a)** Frequency spectrum of the signal; **b)** Signal in the time domain.

- ***Size 4: 60x60***.

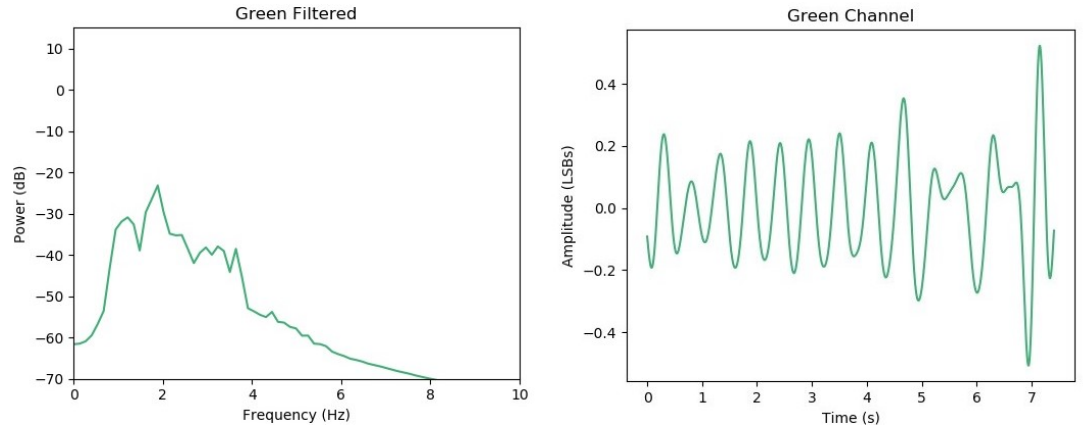

(a) **(b)**

Figure 3.22: Signal of the green channel calculated for the 60x60 ROI size. **a)** Frequency spectrum of the signal; **b)** Signal in the time domain.

- ***Size 5: 40x40***.

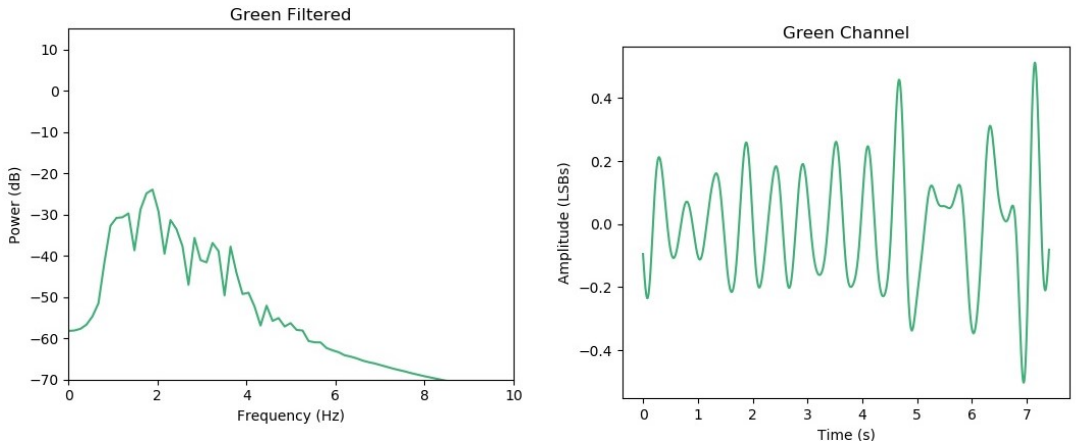

(a) **(b)**

Figure 3.23: Signal of the green channel calculated for the 40x40 ROI Size. **a)** Frequency spectrum of the signal; **b)** Signal in the time domain.

- ***Size 6: 20x20***.

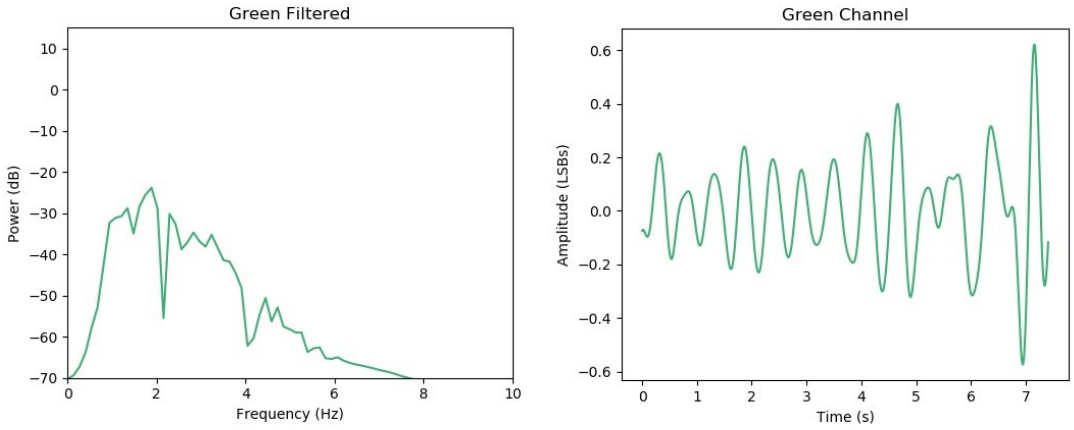

(a) **(b)**

Figure 3.24: Signal of the green channel calculated for the 20x20 ROI Size. **a)** Frequency spectrum of the signal; **b)** Signal in the time domain.

3.3 Depth techniques

3.3.1 ROI location

As shown in figure 3.25 and figure 3.32, there are differences in the signals obtained from the two chosen zones. Table 3.12 and table 3.13 show the results of *ROI analysis* where APP is the peak to peak amplitude, HP_1 is the highest peak in the frequency spectrum, HP_2 is the second highest peak in the frequency spectrum, NFP is the noise floor power, is the difference between the two highest peaks and SNR is the *signal-to-noise ratio*. In the time domain it can be seen how the signal obtained in the abdomen follows a sinusoidal pattern while the signal obtained in the chest area shows components that significantly deform the signal. Most likely, these more frequent components are part of the movement of the heart in the chest at each heartbeat. Visually, these differences were expected since, when reproducing the videos, it was observed that the zone that larger movement manifested was the abdominal zone. In terms of the results obtained in the analysis, there are large differences. The amplitude of the signal in the abdomen is much greater than in the chest area. For this reason and because both the difference between highest peaks and the *signal-to-noise ratio* are also higher, the abdominal area has been chosen as the best region.

ROI Location	**APP** (LSBs)	**HP**$_1$ (dB)	**HP**$_1$ (Hz)	**HP**$_2$ (dB)	**HP**$_2$ (Hz)	**NFP** (dB)
Chest	4.28	-8.77	0.79	-9.78	0.57	-35.98
Abdomen	9.77	-0.36	0.56	-3.11	0.71	-34.50

Table 3.12: Results of the ROI location assessment.

ROI Location	**ΔHP** (dB)	**SNR** (dB)
Chest	1.01	27.21
Abdomen	2.74	34.14

Table 3.13: Results of the ROI location assessment.

- ***Chest***.

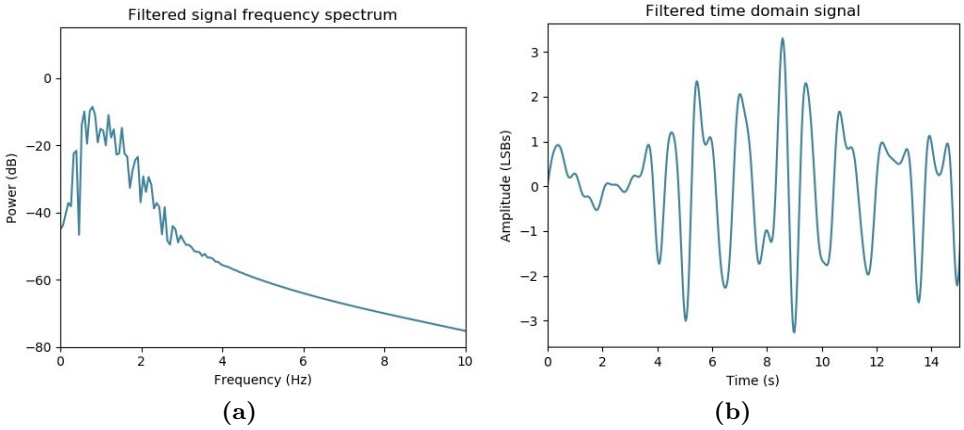

(a) **(b)**

Figure 3.25: Obtained signal from the chest. **a)** Frequency spectrum of the signal; **b)** Time domain signal.

- ***Abdomen***.

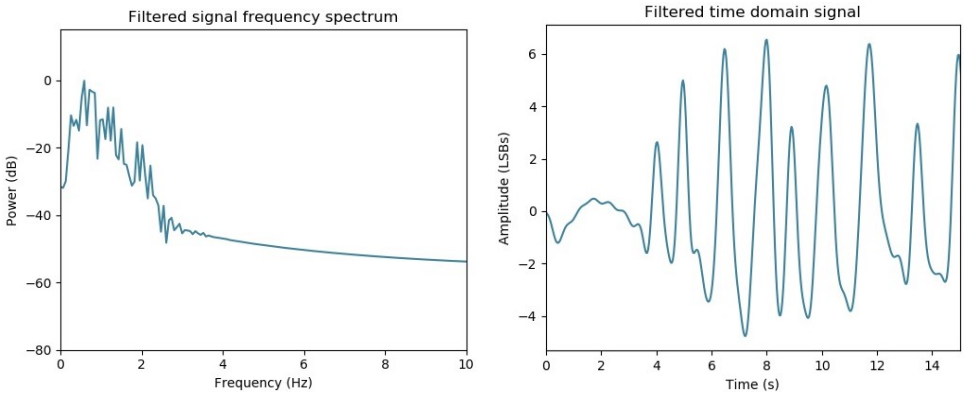

(a) **(b)**

Figure 3.26: Obtained signal from the abdomen. **a)** Frequency spectrum of the signal; **b)** Time domain signal.

3.3.2 ROI Size

The results of the analysis of the most suitable ROI size and in which the best results have been obtained are shown in table 3.14 and table 3.15. It is quite difficult to choose the best option because the results are very tight. The *ROI* in which larger signal amplitude is obtained is *50x50*, however the difference between the two highest peaks is smaller than in other *ROIs*. The largest *ROI* is the one in which the greatest difference between the two highest peaks has been obtained. In addition, in this *ROI*, the value of the *signal-to-noise ratio* and the value of the *standard deviation* have been considered adequate. On the other hand, as discussed in the methodology section, the acquisition frequency in this application is 30 frames per second, so the volume of data was much lower than in the HR signal extraction part and less critical and demanding. Therefore, the most suitable *ROI* size for the extraction of the BR is *200x200* pixels.

ROI Size (pixels)	**APP** (LSBs)	**HP**$_1$ (dB)	**HP**$_1$ (Hz)	**HP**$_2$ (dB)	**HP**$_2$ (Hz)	**NFP** (dB)
400x400	7.92	-5.31	0.56	-6.53	0.73	-37.76
300x300	8.61	-3.05	0.53	-3.61	0.79	-36.48
200x200	9.77	-0.36	0.56	-3.11	0.71	-34.50
100x100	11.16	-0.58	0.54	-2.15	0.81	-32.93
50x50	13.14	-2.26	0.58	-3.27	0.79	-28.39
20x20	7.74	-6.19	0.79	-6.64	0.58	-33.01

Table 3.14: Results of the ROI size assessment.

ROI Size (pixels)	**ΔHP** (dB)	**SNR** (dB)	**SD** (LSBs)
400x400	1.01	26.13	6.1
300x300	0.56	33.43	5.32
200x200	2.75	34.14	5.21
100x100	1.57	32.35	5.59
50x50	1.01	26.13	6.26
20x20	1.01	26.13	4.39

Table 3.15: Results of the ROI size assessment.

- ***Size: 400x400***.

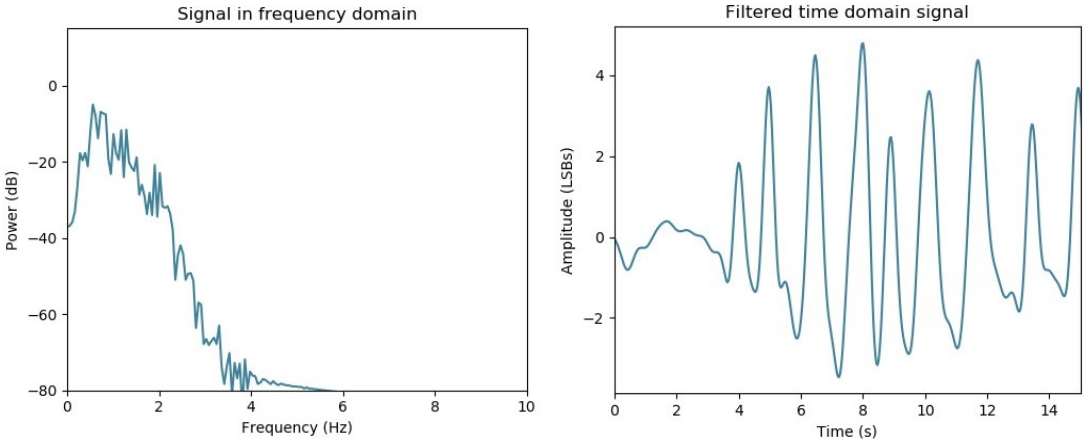

(a) **(b)**

Figure 3.27: Obtained signal from the abdomen ROI (400x400). **a)** Frequency spectrum of the signal; **b)** Time domain signal.

- ***Size: 300x300***.

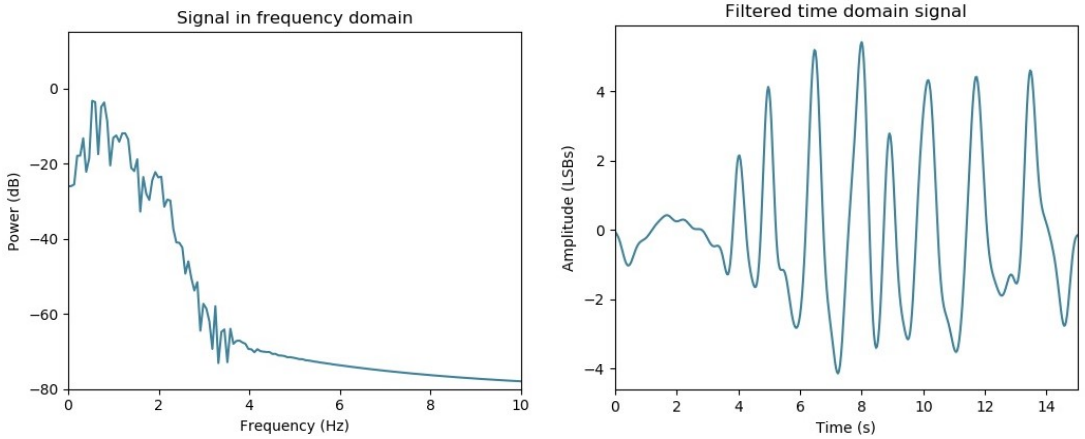

(a) **(b)**

Figure 3.28: Obtained signal from the abdomen ROI (300x300). **a)** Frequency spectrum of the signal; **b)** Time domain signal.

- ***Size: 200x200***.

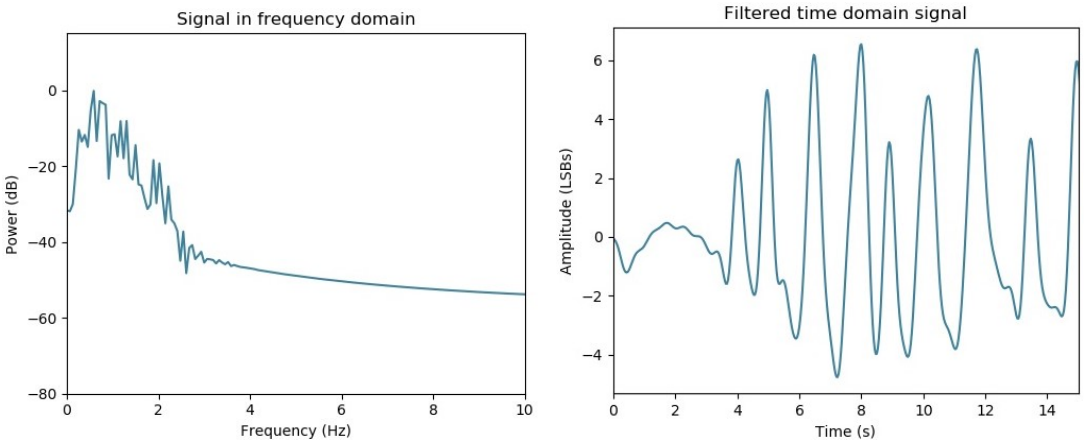

(a) **(b)**

Figure 3.29: Obtained signal from the abdomen ROI (200x200). **a)** Frequency spectrum of the signal; **b)** Time domain signal.

- ***Size: 100x100***.

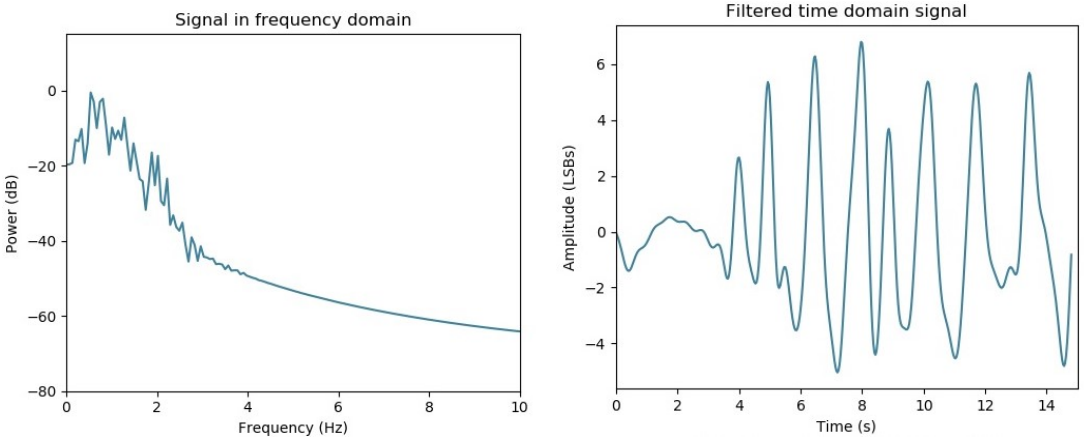

(a) **(b)**

Figure 3.30: Obtained signal from the abdomen ROI (100x100). **a)** Frequency spectrum of the signal; **b)** Time domain signal.

- ***Size: 50x50***.

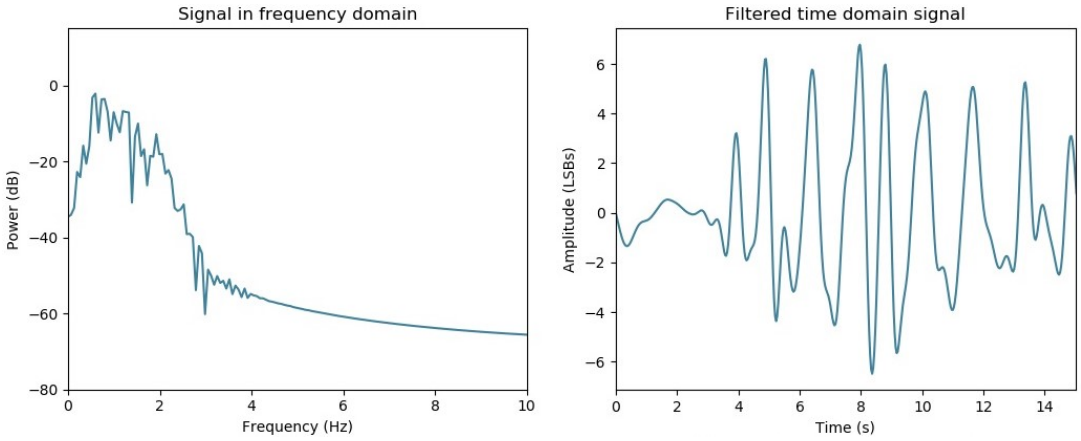

(a) **(b)**

Figure 3.31: Obtained signal from the abdomen ROI (50x50). **a)** Frequency spectrum of the signal; **b)** Time domain signal.

- ***Size: 20x20***.

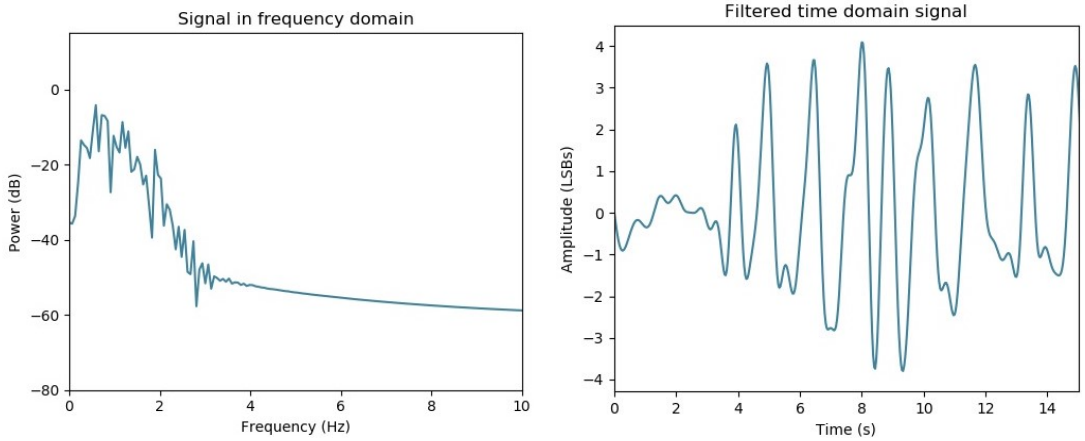

(a) **(b)**

Figure 3.32: Obtained signal from the abdomen ROI (20x20). **a)** Frequency spectrum of the signal; **b)** Signal in the time domain.

Chapter 4

Conclusions

In general terms

The main objectives defined at the beginning of the development of this work have been accomplished. A non-intrusive monitoring system has been proposed that is capable of obtaining the HR and the breathe rate of a neonate in a non-intrusive way. On the one hand, the system has been designed in such a way that HR is obtained from one of the two cameras at 200 frames per second. It has been demonstrated that the optimal region of interest is a 80x80 pixel area in the chest, close to the heart. On the other hand, the system has been designed in such a way that breathe rate can be extracted with the operation of both cameras at 30 frames per second. It has been demonstrated that the optimal region of interest is a 200x200 pixel area in the abdomen.

Being able to extract signals from which it is possible to extract relevant parameters in diagnostic tasks demonstrates that it is possible to design and implement increasingly less intrusive devices for patient monitoring. This is key for both patients and doctors as stress levels in hospitals can be very high. Working on systems where there is no contact with patients may lead to the reduction of such stress and improve the mobility of patients and doctors. During the development of this work several visits were made to the *Neonatology Intensive Care Unit*. In this unit the level of demand and stress are maximum since there are patients with just days of life and sometimes in a very critical situation. In the personal and professional spheres, working in this unit has led to the acquisition of experience in stressful environments. This project was developed with the aim of demonstrating and defining the necessary techniques to be used for non-intrusive monitoring of neonates. All this, so that in the future, can be applied to studies with large population samples.

With respect to hardware, two conventional cameras have been used. This has shown that no high-end cameras are needed to extract HR and breathing signals. In addition, the materials used to build the mechanical modular structure for the prototype were also conventional and easily accessible. Proposing a modular design caused a decrease in costs.

All the applications were developed in *Python*. The main motivation that led to the use of this programming language is that, compared to other alternatives such as *Matlab*, it has an open

source license. This made licensing easier and reduced software costs. In addition, it served as a learning and experience acquisition.

Calibration experiments

The difficulties found in certain areas of the body surface of the neonates with regard to the obtained signals led to the perform several calibration experiments. This was done with the intention of correcting the obtained images if needed. For this reason it was decided to make the study of linearity and homogeneity.

On the one hand, the study of the linearity of the cameras served to demonstrate that it was not essential but advisable to wait for the cameras to warm up. The color level in the cameras took some five minutes to settle. However, the differences between maximum and minimum level of the output signal remained constant and the noise level was within an acceptable range.

On the other hand, the study of the homogeneity in the image made with the integrating sphere tried to identify if the captured image had patterns of noise or non-homogeneous elements under the conditions of a perfectly homogeneous surface. This experiment was used to verify that the cameras offered the expected performance.

Color & Depth techniques

Fulfilling the objectives set at the beginning of this work, it has been demonstrated that using both color techniques and depth mapping techniques we can extract vital signs that are key in the diagnosis of many diseases. The respiratory signal was easier to extract. This was due to the fact that the movement caused by the action of breathing is a signal of great magnitude. Moreover, it is also visible to the naked eye. The cardiac signal was more complicated to extract depending on which areas of the body. As has been demonstrated, if the studied area was close to the heart, the results were better and a distinguishable and measurable signal was obtained. On the other hand, if the studied area was away from the heart, the results were significantly worse. The fact of being able to extract information related to HR as well as respiratory rate opens the doors to the field of analysis of the variability of these parameters. Furthermore, the fact that these techniques have been applied in delicate environments such as Neonatology demonstrates that this type of system can be useful not only at home but also in hospitals.

Limitations

Some limitations especially hampered the normal development of acquiring tasks. Firstly, our initial approach to the use of the monitoring system in the cribs or nests of the Neonatology Intensive Care Unit was limited by the disposition of the neonate. We were informed that certain neonates are covered above the head to such an extent that they sometimes cover the entire body surface. It should be remembered that for the application of HR extraction it was necessary to analyze a small piece of body surface. In addition, the blankets used to provide warmth to the newborn were large in size and had great slack. This made it difficult to extract respiration-related information. Therefore, processing of the videos acquired in the nests had to be discarded, at least for the experimental part of the development of the proposed system. Secondly, the volume of data was especially large during the acquisition of videos to extract information related to HR.

This led to a limitation of acquisition time not being as strict in the videos acquired to extract the breathing signal. Thirdly, light conditions were variable depending on weather conditions or the time of day they were in. In general, it was preferred that newborns did not have artificial light, so sunlight coming in from the windows was enough. Artificial light was only used if conditions required it or if the intensity of sunlight was dimmed during the evening. Therefore, the acquisition tasks with our system focused on acquiring images of those newborns who were in incubators. The incubators provided both mechanical stability and absence of interfering objects in the field of view of the cameras. As for the newborns in the cribs, the system was defined as useful for transient or eventual monitoring in which the baby would be in a favorable position to measure and extract the characteristics. In addition, in order to acquire images of the neonates and especially their faces, a consent document had to be defined and written. This document had to be signed by the parents or legal representatives of the newborn; in some cases the parents or legal representatives refused to sign the document, which limited the number of newborns to work with. The document can be found in Annexes.

With respect to the signals that could be processed and due to the limit in the time of acquisition previously commented, consequently there were short registers on which to make studies or to extract specific conclusions. The records showed correct information, but the study of frequency variability would be limited.

Future challenges

As for the future challenges related to this system, both hardware and software aspects have been taken into account. On the one hand, the fact that the structure is placed on top of the incubator is a circumstance that somewhat limits the space for nurses. Therefore, it would be necessary to design a structure that would be able to hold the cameras in an oblique plane and that would not be in contact with the incubator. This structure would either be attached to the trolley transporting the incubator or it would be attached with a base on the floor. The design should always be approached from a point of view of not obstructing the staff working in the hospital. On the other hand, regarding the software, it would be essential to develop a real-time application that could show constant feedback with doctors. In this way they could know data about the patient's condition in terms of heart rhythms or breathing rhythms. When showing feedback, one should be cautious as to the amount of information that should be offered, since an excess of information in terms of text messages could stress or alarm patients. In case of offering text messages, it would be recommended to show only technical information or information related to the status of the device (power, connections ...). As for data, storing records in a device may not be sustainable over time due to memory issues. Proposing a data storage in the cloud could be interesting. Perhaps in this way both parents or legal representatives of newborns and other adult patients could access their information.

In addition to these aspects, this type of system could be adapted to other environments such as nursing homes or other hospital units so that it would not only be used for newborns. The fact that it is non-intrusive suggests that it may be adaptable and comfortable in a wide range of environments.

Chapter 5

Budget and Planning

This section details the budget and the planning defined for the execution of this project. Table 5.1 details labor, needed hardware and all software licenses used during the design and development of the system. In the next page the scheduling of the execution of the project is presented as a Gantt chart.

Resources and costs				
AREA	**CONCEPT**	**UNITS**	**COST/Unit (€)**	**COST (€)**
Labor	Engineer	8 (months)	36,000 (per year)	24,000
Hardware	Computer	1	1,700	1,700
	Video-cameras	2	390	780
	Micro B 3.0-USB Cable	2	30	60
	Mechanical structure	1	167.67	167.67
Software	Latex license	1	-	-
	Overleaf license	2	7.99	15.98
	Microsoft license	1	69	69
	Python license	1	-	-
	Pycharm license	1	-	-
	Matlab license	1	800	800
	Pylon Viewer license	1	-	-
			TOTAL COST	27,592.65

Table 5.1: Project budget.

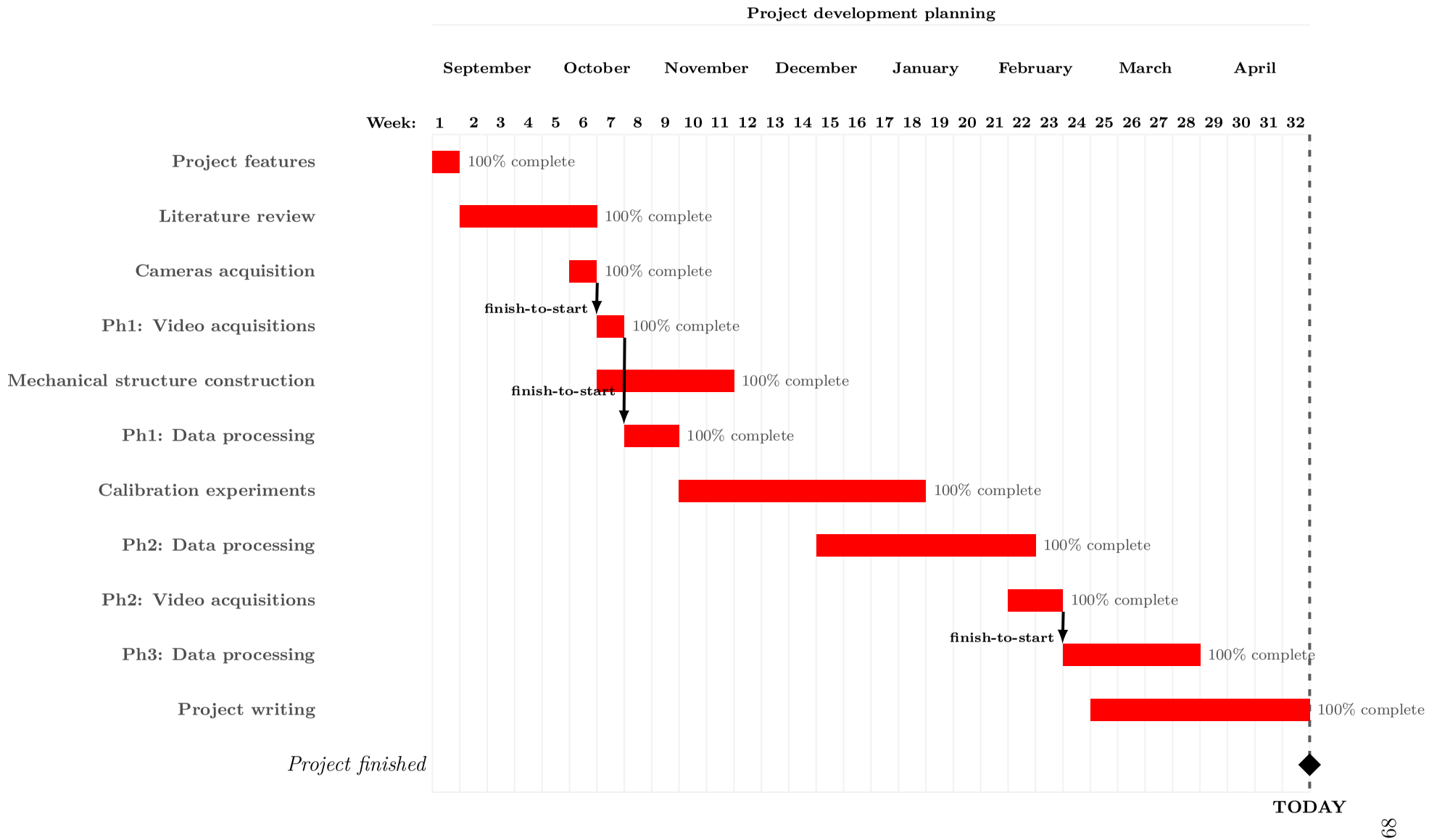
Project development planning
September
October
November
December
January
February
March
April
Week: 1 2 3 4 5 6 7 8 9 10 11 12 13 14 15 16 17 18 19 20 21 22 23 24 25 26 27 28 29 30 31 32
Project features
100% complete
Literature review
100% complete
Cameras acquisition
100% complete
finish-to-start
Ph1: Video acquisitions
100% complete
Mechanical structure construction
finish-to-start
100% complete
Ph1: Data processing
100% complete
Calibration experiments
100% complete
Ph2: Data processing
100% complete
Ph2: Video acquisitions
100% complete
finish-to-start
Ph3: Data processing
100% complete
Project writing
100% complete
Project finished
TODAY

Part II

Annexes

Drawings

In this section we expose the mechanical structure drawings. It contain the three views of the mechanical structure and the isometric viewpoint. The document starts in the next page.

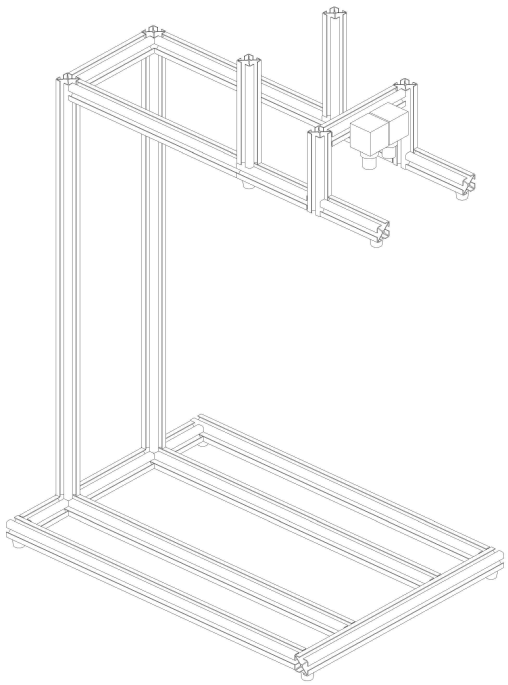

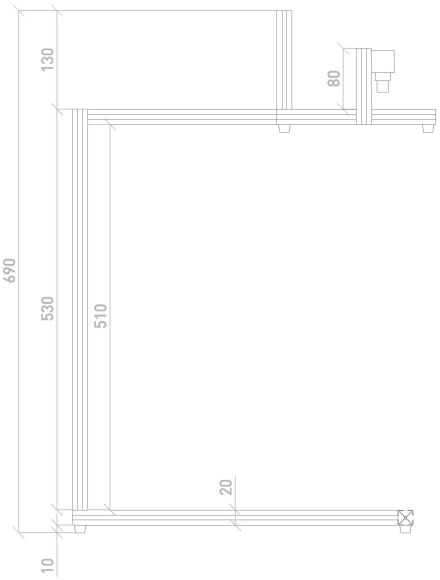
130
80
690
530
510
20
10


320

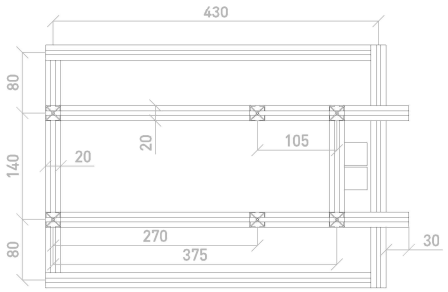
430
80
20
105
140
20
270
30
80
375

Informed Consent Document

In this section we present the Informed Consent Document that parents or legal representatives of the neonates had to sign. It starts in the next page.

Comité Ético de Investigación con Medicamentos

Consorcio Hospital General Universitario

Valencia

Valencia 15 de Octubre de 2018

Estimados Señores,

Se adjuntan los cambios solicitados del proyecto: "Estudio de un sistema para la monitorización continua y sin contacto de constantes vitales en recién nacidos: El caso de la sepsis neonatal"

1. En LA HOJA DE INFORMACIÓN + CONSENTIMIENTO INFORMADO

En el apartado de confidencialidad tiene que completarse los siguientes datos

1-Sus datos personales serán tratados de manera confidencial, y se procesarán conforme a la Ley Orgánica de Protección de Datos de Carácter Personal (15/1999, del 13 de Diciembre). El tratamiento de toda la información obtenida en el estudio está regulado por las leyes nacionales e internacionales de datos y de confidencialidad.

- Se ha introducido en el apartado de confidencialidad.

2- Debe de utilizarse como hoja de consentimiento la referida como consentimiento informado del representante legal pero suprimiendo el apartado en mi presencia se ha dado toda la información pertinente adaptada a su nivel de entendimiento y está de acuerdo en participar.

- Se ha suprimido dicho apartado

3- En relación con la obtención de imágenes se debe de acompañar de un documento específico de consentimiento informado en la realización de video-filmación y toma de imágenes del CHGUV.

- Se incluye el consentimiento del CHGUV con Instrucción 5/18 para la realización de video-filmación y toma de imágenes.

Un cordial saludo

Empar Lurbe Ferrer

Jefa de Servicio de Pediatría
Investigadora Principal

IMPRESO DE INFORMACIÓN Y CONSENTIMIENTO INFORMADO

TÍTULO: Estudio de un sistema para la monitorización continua y sin contacto, de constantes vitales en recién nacidos: El caso de la sepsis neonatal.

INVESTIGADOR PRINCIPAL

Dra. Dña. Empar Lurbe Ferrer

OBJETIVOS

El objetivo principal del presente proyecto es estudiar la viabilidad técnica de desarrollar e implementar un sistema para la monitorización de constantes vitales y comportamiento sin contacto y de este modo mejorar el seguimiento clínico de niños ingresados por sepsis en la sala de Neonatos y Cuidados Intermedios del Servicio de Pediatría del Consorcio Hospital General Universitario de Valencia**.**

DESCRIPCIÓN DEL ESTUDIO

El periodo neonatal supone una etapa crítica de la vida en la que es fundamental la detección precoz de una serie de enfermedades que pueden debutar con un cuadro grave, con consecuencias graves y en algunos casos con resultado de muerte. Es por ello que en este grupo de edad cobra especial relevancia detectar de forma precoz signos de alarma que orienten a la presencia de enfermedades. Además es fundamental disponer de pruebas que no supongan exploraciones invasivas al recién nacido, en otras palabras evitar en lo posible extracciones de sangre. Dentro de este contexto se encuentra la sepsis neonatal que puede tener consecuencias graves a corto y largo plazo. En este sentido se ha demostrado para el diagnóstico precoz y seguimiento de la sepsis la utilidad del estudio de los cambios en la frecuencia de los latidos del corazón así como la frecuencia de las respiraciones. El identificar estas alteraciones de forma precoz permite establecer más pronto el tratamiento y mejorar la evolución a corto y largo plazo. El disponer de métodos no invasivos que nos ayuden a la detección precoz es fundamental con el fin de mejorar el bienestar del niño y la familia.

El estudio se centra en conocer si por medio de la obtención de imágenes podemos detectar la frecuencia de los latidos del corazón y sus cambios así como la frecuencia de las respiraciones. ¿Cómo se consiguen estas imágenes? Dispondremos de 2 cámaras especiales que estarán durante un periodo de entre 30-60 minutos adquiriendo imágenes solamente del pecho del recién nacido. Posteriormente se aplicaran cálculos matemáticos que nos permitirán obtener la información de si el número de latidos del corazón así como la frecuencia de las respiraciones es normal. La obtención de imágenes será solamente de la zona correspondiente al pecho de ahí que en ningún momento permitirá identificar al niño. Solamente estarán disponibles para el personal sanitario asociado al proyecto. Todo el proceso de obtener los resultados se llevará a cabo en el Servicio de Pediatría de nuestro Hospital.

¿Dónde estará el recién nacido mientras se lleve a cabo la obtención de las imágenes? Permanecerá en el mismo sitio, bien en la incubadora o en la cuna.

Para poder participar en este programa, es necesario tener el consentimiento por parte de los padres o tutores legales. Si Ud. está de acuerdo, libremente firme el consentimiento de participación en este estudio que para este fin se ha añadido al final de este documento.

RIESGOS Y BENEFICIOS

No existen riesgos para los pacientes participantes.

Con su participación en este estudio, usted está contribuyendo en estudiar la posibilidad de desarrollar un nuevo sistema de obtener signos vitales, latidos del corazón y frecuencia de las respiraciones sin contacto con el paciente. Ello puede suponer un avance importante en la atención a los recién nacidos ingresados en la sala de Neonatos o Cuidados Intermedios del Servicio de Pediatría del Consorcio Hospital General Universitario de Valencia.

PARTICIPACIÓN EN EL ESTUDIO

Si acepta que su hij@ participe en el estudio supondrá la autorización para que su hij@ en paralelo al control de constantes, como la frecuencia de los latidos cardiacos o la respiratoria mediante monitores convencionales, se obtenga durante un periodo de entre 30-60 minutos la frecuencia de los latidos cardiacos y la respiratoria mediante imágenes y sin contacto físico. Las imágenes serán almacenadas y anonimizadas y los resultados se compararan con los obtenidos a través de los monitores convencionales.

También consistirá en autorizar el obtener datos de la historia clínica tanto del recién nacido como de la madre. Toda esta información solamente se empleará con fines de avanzar en el diagnóstico precoz de enfermedades que debutando en el periodo neonatal pueden comprometer la vida del recién nacido o bien producir secuelas. Todos los datos obtenidos se trataran conforme a la legislación vigente.

Su participación en este estudio es totalmente voluntaria y no recibirá remuneración alguna. Ustedes pueden decidir libremente retirarse del estudio en cualquier momento, sin que ello suponga ninguna modificación en la calidad de la atención al recién nacido.

CONFIDENCIALIDAD

Toda la información obtenida será confidencial, los datos recogidos se introducirán, por el Equipo investigador, en una base de datos para realizar el estudio de los resultados. Los datos se anonimizaran, es decir, el nombre no aparecerá en ningún documento del estudio, sólo se le asignará un número. En ningún caso se le identificará en las publicaciones que puedan realizarse con los resultados del estudio. Sin embargo, esta información estará disponible y podrá ser revisada por el Comité Ético de Investigación Clínica de este Hospital así como por organismos gubernamentales competentes si así lo requieren.

El estudio se realizará asegurando el cumplimiento de normas éticas y legales vigentes (Declaración de Helsinki) y ha sido aprobado por el Comité Ético de Investigación Clínica del Consorcio Hospital General Universitario de Valencia.

Si tiene alguna duda o no entiende este texto consulte antes de firmar el documento con la Dra. Empar Lurbe, Jefa del Servicio de Pediatría con nº de teléfono 963131800, ext 437358 que es el médico responsable de esta investigación y le puede preguntar cualquier duda o que tenga relacionada con este estudio. Si está de acuerdo firme este consentimiento. Se le entregará una copia.

Sus datos personales serán tratados de manera confidencial, y se procesarán conforme a la Ley orgánica de protección de Datos de Carácter Personal (15/1999, del 13 de diciembre). El Tratamiento de toda la información obtenida en el estudio está regulado por las leyes nacionales e internacionales de datos y de confidencialidad.

Fdo.: Dra. Empar Lurbe Ferrer

Investigador Principal del Proyecto

Jefa del Servicio de Pediatría

Tel: 963131800 Ext:437358

CONSENTIMIENTO INFORMADO DEL REPRESENTANTE LEGAL.

Título del proyecto de investigación: Estudio de un sistema para la monitorización continua y sin contacto de constantes vitales en recién nacidos. El caso de la sepsis neonatal.

Yo, ...

en calidad de: .....

de: .....

He leído la hoja de información anterior.

He podido hacer preguntas sobre el estudio.

He recibido suficiente información sobre el estudio.

He hablado con .....

Comprendo que la participación es voluntaria.

Comprendo que puede mi hij@ puede retirarse del estudio:

- **Cuando quiera.**
- **Sin tener que dar explicaciones.**
- **Sin que esto repercuta en los cuidados médicos al recién nacido.**

Comprendo que este material aparezca en informes y artículos de revista de publicaciones médicas.

Entiendo que:

- **El nombre del recién nacido no será publicado.**
- **El material y resultados obtenidos no será utilizado para publicidad o embalaje.**
- **El material y resultados obtenidos no será utilizado fuera de contexto.**

Y presto mi conformidad con que .....

..... participe en el estudio

Firmado ..... Fecha.....

ORGANO DEL QUE EMANA:	INSTRUCCIÓN:
COMISIÓN DE DIRECCIÓN DEL CONSORCIO HOSPITAL GENERAL UNIVERSITARIO DE VALENCIA	05 / 2018 (AST) **FECHA:** 19/06/2018
ASUNTO:	**DESTINATARIOS:**
INSTRUCCIONES PARA OTORGAR EL CONSENTIMIENTO INFORMADO EN LA REALIZACIÓN DE VIDEO-FILMACIÓN Y TOMA DE IMÁGENES	SERVICIOS ASISTENCIALES DEL DEPARTAMENTO VALENCIA H. GENERAL, ATENCIÓN AL PACIENTE, DIRECCIÓN DE INVESTIGACIÓN Y DOCENCIA Y GABINETE DE COMUNICACIÓN

La video-filmación y toma de imágenes se ha mostrado como un método útil para el estudio de diferentes patologías, así como método de aprendizaje y corrección de errores durante la entrevista clínica, entre otras cuestiones. Esta técnica permite además el análisis más detallado de la sintomatología y la evaluación de su evolución y de la enfermedad, bien por su evolución temporal o por las modificaciones debidas al tratamiento.

Por otra parte, los datos grabados pueden ser analizados y discutidos con otros expertos en actos científicos, conferencias y congresos, facilitando no solo un mejor conocimiento de la enfermedad sino también la recogida de ideas nuevas acerca de la patología a analizar. Además, la posibilidad de recoger en imágenes los diferentes datos de un paciente es de gran utilidad para la formación de profesionales y para la docencia de la medicina.

Con el fin de ordenar los circuitos para la obtención de estos archivos de imágenes, preservando la identidad y el anonimato del usuario en todo momento y garantizando el cumplimento de todas las medidas de seguridad que exige la normativa actual se aprueba la presente Instrucción.

Primera.

Obtención del consentimiento

1. El profesional sanitario (facultativo o de enfermería) decide realizar una grabación que involucre a algún paciente por los motivos anteriormente mencionados.
2. El profesional informa al paciente de la posibilidad de realizar una grabación de vídeo o toma de imágenes en relación con su patología (lesiones, intervenciones quirúrgicas, técnicas diagnósticas, evolución...) o para su uso en actos científicos, docentes o de investigación.
3. Si el paciente acepta que se realice la filmación o tomas de imágenes, se le entrega el modelo de consentimiento (modelo anexo I) para que lo revise y lo firme.
4. El consentimiento se remitirá al archivo para su escaneo e incorporación a la historia clínica electrónica.

Segunda.

Obtención de las imágenes

1. En el caso de que las imágenes se obtengan por medio de empresas externas, el profesional responsable se asegurará de que la empresa firme el correspondiente compromiso de confidencialidad (Anexo II) una vez obtenido el consentimiento del paciente de acuerdo al punto anterior.

2. En la toma de imágenes se deberá eliminar los signos identificativos, difuminando los rasgos faciales que los hagan reconocibles.

3. La filmación solo se podrá iniciar una vez se disponga de los modelos Anexo I y en caso de empresas externas además el Anexo II, correctamente cumplimentados y firmados.

Tercera.

Uso y conservación de las imágenes

1. Los datos grabados podrán ser utilizados para diferentes actos científicos, docentes o de investigación facilitando la formación e información sobre la enfermedad e incluso la investigación sobre la misma.

2. El profesional sanitario correspondiente se hará responsable de la custodia de las imágenes obtenidas según el circuito marcado en esta instrucción.

El Director Gerente

Fdo.: Dr. Enrique Ortega González

ANEXO I

DECLARACIÓN DE CONSENTIMIENTO

NOMBRE DEL PACIENTE:.....
Nº Historia:.....
SIP: .....

ETIQUETA DEL PACIENTE

He sido informado por el Dr./Dra.....adscrito a la unidad/servicio de ..... de la realización de video-filmación y toma de imágenes para la técnica _____ según consta en el consentimiento informado de dicha técnica.

En..... a..... de ..... de 20.....

Nombre del paciente DNI:	Nombre del médico DNI:
Firma del paciente Fecha:	Firma del médico Fecha:

REVOCACIÓN
D.Dña.:....., con DNI/Pasaporte nº:..... D.Dña.:....., con DNI/Pasaporte nº:..... como representante y/o tutor del paciente REVOCO el consentimiento prestado. En..... a..... de ..... de 20..... Firma del paciente/representante y/o tutor

ANEXO II

COMPROMISO DE CONFIDENCIALIDAD Y NO DIVULGACIÓN DE INFORMACIÓN RESERVADA

Yo, _____, con DNI/CIF _____ actuando como representante de _____-_____, cuyo objeto consiste en filmar imágenes en del departamento Valencia-Hospital General, encargadas por:

_____ del centro/servicio/unidad _____, estoy acuerdo con las siguientes disposiciones:

PRIMERA. - Objeto. Mediante el presente acuerdo me obligo a guardar reserva de la información que se me va a proporcionar para la video-filmación y toma de imágenes, tanto de la identidad del paciente como de los comentarios que se hagan mientras realizo la grabación.

SEGUNDA. - Obligación de reserva. En cumplimiento de la obligación deberé:

1. Garantizar la más estricta confidencialidad y advertir de dicho deber de confidencialidad y secreto a cualquier persona que por su relación conmigo deba tener acceso a dicha información para el correcto cumplimiento de sus obligaciones.

2. Abstenerme de reproducir, modificar, hacer pública o divulgar a terceros la información objeto del presente acuerdo.

3. Adoptar, respecto de la información objeto de este acuerdo, las medidas de seguridad que requiere la normativa vigente respecto a los datos de carácter personal y garantizar la confidencialidad y no divulgación de la información entregada para evitar su pérdida, robo o sustracción o utilización no autorizada.

TERCERA. - Indemnización. Me comprometo a resarcir los perjuicios por daño y lucro que llegara a ocasionar la revelación, divulgación, o utilización de la video-filmación y toma de imágenes de cualquier forma distinta al objeto de este acuerdo, ya sea de forma dolosa o por mera negligencia, sin perjuicio de las demás acciones legales que se puedan adoptar.

CUARTA. - Vigencia. El presente acuerdo entrará en vigor en el momento de la firma y su obligación de confidencialidad perdurará mientras la información conserve las características para considerarse confidencial.

Expreso mi conformidad y aceptación de los términos recogidos en el presente documento,

En Valencia, a ..... de ..... de 20.....

Firma: _____

Dirección: _____

Bibliography

Aarts, Ronald M (2004). "Low-complexity tracking and estimation of frequency and amplitude of sinusoids". In: *Digital Signal Processing* 14.4, pp. 372–378 (cit. on p. 31).

AliveCor (n.d.). *AliveCor KardiaMobile ECG*. URL: https://www.alivetec.com/pages/alivecor-heart-monitor (cit. on p. 6).

Aslam, Asra, Mohd Ansari, et al. (2019). "Depth-Map Generation using Pixel Matching in Stereoscopic Pair of Images". In: *arXiv preprint arXiv:1902.03471* (cit. on p. 36).

BASLER (n.d.). *Camera specifications and features: acA1300-200uc - Basler ace*. URL: https://www.baslerweb.com/en/products/cameras/area-scan-cameras/ace/aca1300-200uc/#tab=specs (cit. on p. 13).

Basler (n.d.). *Basler acA3000 - 200 uc Datasheet*. URL: http://www.qataa.com/upLoad/file/20180209/15181627172137876.pdf (cit. on p. 18).

Cochran, William T et al. (1967). "What is the fast Fourier transform?" In: *Proceedings of the IEEE* 55.10, pp. 1664–1674 (cit. on p. 31).

Flenady and Dwyer (2016). "Accurate respiratory rates count: So should you!" In: *Australasian Emergency Nursing Journal 20 (2017)*, pp. 45–47 (cit. on p. 5).

Foroozan, Foroohar, Madhan Mohan, and Jian Shu Wu (2018). "Robust Beat-To-Beat Detection Algorithm for Pulse Rate Variability Analysis from Wrist Photoplethysmography Signals". In: *2018 IEEE International Conference on Acoustics, Speech and Signal Processing (ICASSP)*. IEEE, pp. 2136–2140 (cit. on p. 7).

Guyton, Arthur C. and John E. Hall (2011a). *Textbook of Medical Physiology*. Saunders by Elsevier. Chap. 9 (cit. on p. 4).

— (2011b). *Textbook of Medical Physiology*. Saunders by Elsevier. Chap. 13 (cit. on p. 4).

Hirschmuller, Heiko (2007). "Stereo processing by semiglobal matching and mutual information". In: *IEEE Transactions on pattern analysis and machine intelligence* 30.2, pp. 328–341 (cit. on p. 36).

Jubran, Amal (2015). "Pulse oximetry". In: *Critical Care* (cit. on p. 23).

Kliegman, R.M. (2015). *Nelson Textbook of Pediatrics*. Elsevier. Chap. 3 (cit. on pp. 3–5).

Kutlu, Yakup and Damla Kuntalp (2010). "Feature extraction for ECG heartbeats using higher order statistics of WPD coefficients". In: *computer methods and programs in biomedicine* (cit. on p. 6).

Labsphere (n.d.[a]). *IHLS, EHLS and IRLS Series External Halogen Light Sources*. URL: `http://host.web-print-design.com/labsphere/products/integrating_sphere_light_sources/halogen_light_sources.htm` (cit. on p. 18).

— (n.d.[b]). *Uniform Radiance Spheres for the Test and Calibration of Imaging and Non-imaging Devices*. URL: `http://www.labsphere.com.cn/admin/UploadFiles/product/201481215325636.pdf` (cit. on p. 17).

Maschal Jr, Robert A et al. (2010). *Review of Bayer pattern color filter array (CFA) demosaicing with new quality assessment algorithms*. Tech. rep. Army Research Lab Adelphi Md Sensors and Electron Devices Directorate (cit. on p. 22).

Mejía and Daza (2011). "Semiologia neonatal". In: *Gastrohnup* (cit. on p. 37).

Motedis (n.d.). *Motedis shop. Your online shop for aluminium profiles and accessories*. URL: `https://www.motedis.es/shop/index.php` (cit. on p. 15).

Nishad and Dr. R.Manicka Chezian (2013). "Various colour spaces and colour space conversion". In: *Journal of Global Research in Computer Science* 4.1, pp. 44–48 (cit. on p. 22).

Norvang, LT et al. (1997). "Skin pigmentation characterized by visible reflectance measurements". In: *Lasers in Medical Science* 12.2, pp. 99–112 (cit. on p. 23).

Ontario, Health Quality et al. (2017). "Long-Term Continuous Ambulatory ECG Monitors and External Cardiac Loop Recorders for Cardiac Arrhythmia: A Health Technology Assessment". In: *Ontario health technology assessment series* 17.1, p. 1 (cit. on p. 6).

Pan and Tompkins (1985). "A real-time QRS detection algorithm". In: *IEEE Trans. Biomed. Eng* 32.3, pp. 230–236 (cit. on p. 6).

Park, Sung-Bin et al. (2008). "An improved algorithm for respiration signal extraction from electrocardiogram measured by conductive textile electrodes using instantaneous frequency estimation". In: *Medical & biological engineering & computing* 46.2, pp. 147–158 (cit. on p. 6).

Poh, Ming-Zher, Daniel J McDuff, and Rosalind W Picard (2010). "Non-contact, automated cardiac pulse measurements using video imaging and blind source separation." In: *Optics express* 18.10, pp. 10762–10774 (cit. on p. 7).

Russian, PhD (2015). *The muscles you never think about until they stop working*. URL: `https://www.elsevier.com/connect/the-muscles-you-never-think-about-until-they-stop-working` (cit. on p. 5).

Spodick, David H (1992). *Normal sinus heart rate: sinus tachycardia and sinus bradycardia redefined.* (Cit. on p. 4).

Steinberg, Jonathan S et al. (1992). "Predicting arrhythmic events after acute myocardial infarction using the signal-averaged electrocardiogram". In: *The American journal of cardiology* 69.1, pp. 13–21 (cit. on p. 6).

Tamura, Toshiyo et al. (2014). "Wearable photoplethysmographic sensorspast and present". In: *Electronics* 3.2, pp. 282–302 (cit. on p. 7).

Valderas, MT et al. (2015). "Extracción de la señal de respiración a partir del electrocardiograma". In: *Actas de las XXXVI Jornadas de Automática*, pp. 759–765 (cit. on pp. 3, 6).

Vision, Nerian (2019). *Lens Focal Length and Stereo Baseline Calculator*. URL: `https://nerian.com/support/resources/calculator/` (visited on 01/24/2019) (cit. on pp. 11, 12).

WHO (n.d.). *World Health Organization - Management of newborn illness and complications*. URL: `https://www.who.int/maternal_child_adolescent/newborns/management_illness_complications/en/` (cit. on p. 3).

Wu, Hao-Yu et al. (2012). "Eulerian video magnification for revealing subtle changes in the world". In: (cit. on p. 8).